INFORMATION TO USERS

This manuscript has been reproduced from the microfilm master. UMI films the text directly from the original or copy submitted. Thus, some thesis and dissertation copies are in typewriter face, while others may be from any type of computer printer.

The quality of this reproduction is dependent upon the quality of the copy submitted. Broken or indistinct print, colored or poor quality illustrations and photographs, print bleedthrough, substandard margins, and improper alignment can adversely affect reproduction.

In the unlikely event that the author did not send UMI a complete manuscript and there are missing pages, these will be noted. Also, if unauthorized copyright material had to be removed, a note will indicate the deletion.

Oversize materials (e.g., maps, drawings, charts) are reproduced by sectioning the original, beginning at the upper left-hand corner and continuing from left to right in equal sections with small overlaps. Each original is also photographed in one exposure and is included in reduced form at the back of the book.

Photographs included in the original manuscript have been reproduced xerographically in this copy. Higher quality 6" x 9" black and white photographic prints are available for any photographs or illustrations appearing in this copy for an additional charge. Contact UMI directly to order.

UMI

A Bell & Howell Information Company
300 North Zeeb Road, Ann Arbor, MI 48106-1346 USA
313/761-4700 800/521-0600

7

Phase Locking in Laser Arrays

by

Jingwen Xu

A dissertation submitted to the Graduate Faculty in
Physics in partial fulfillment of the requirements
of the degree of Doctor of Philosophy,
The City University of New York.

1995

UMI Number: 9530931

UMI
300 North Zeeb Road
Ann Arbor, MI 48103

This manuscript has been read and accepted for the Graduate Faculty in Physics in satisfaction of the dissertation requirement for the degree of Doctor of Philosophy.

4/4/95
Date

Chair of Examining Committee

4/6/95
Date

Joseph B. Krieger
Executive Officer

Professor Janos Bergou

Professor Mark Hillery

Professor P. P. Ho

Professor Tycho Sleator

Supervisory Committee

The City University of New York

Abstract

Phase locking in laser arrays
by
Jingwen Xu

Advisor: Professor Ying-chih Chen

A two-element laser array is used as a simple experimental model for studying the physics of phase locking in evanescent-coupled laser arrays. The array consists of two closely-spaced lasing filaments created in a monolithic Nd:YAG etalon by photo-pumping. With photo-pumping, the key parameters of the laser array can be controlled and continuously varied for exploring the various phenomena of phase locking over a wide range of coupling strength for comparison with previous theoretical calculations. The study revealed discrepancies between the experimental results and previous theoretical predictions based on the coupled-oscillator model. These discrepancies include: 1) Contrary to previous predictions of slow locking process and the existence of instability, the time of phase locking is observed to be as fast as the lasing process without a slow evolutionary process. There is also no optical instability in the presence of a frequency detuning between the two elements. 2) The experimentally measured frequency detuning for phase locking is much larger than the theoretical predictions. There exists a complex modal patterns in the vicinity of the boundary of phase locking which can not be synthesized by the coupled-oscillator model. The fast locking and lack of instability can be attributed to the presence of a large imaginary part of the coupling strength not properly taking into account in previous theoretical modeling. However, the range of phase locking and the complex transitional behavior can not be explained by the coupled-oscillator model. Our analysis shows that a two-element laser array is not a two-mode system, but can posses numerous eigenmodes, each having a different frequency. For a given frequency, the resonance condition in each branch determines the field strength in that branch and the modal pattern for the composite waveguide can be calculated numerically. The lasing mode is the one with the highest modal gain. With this new understanding, we have successfully explained the complex modal patterns in the vicinity of the transition region and the magnitude of frequency detuning tolerance for phase locking. Another important implication of our new understanding is that the temporal behavior of the laser array can not be synthesized by the linear superposition of the temporal behavior of the individual elements because the dynamics in the laser array is not a deterministic process.

Acknowledgments

I would like to thank my advisor, Professor Ying-chih Chen for his encouragement, guidance and support. His devotion to physics and patience in teaching will serve as an example forever in my career.

Many thanks go to my colleagues, Dr. Gang Yao, Dr. Pei Wang, Professor Shouhuan Zhou, and Professor Shiqun Li. It is a real pleasure to work with them. Their humor and kindness made the laboratory a really enjoyable environment to stay.

I would also like to express my thanks to Hunter College Physics Department staff for providing me a lot of help.

I would like to thank my parents for their constant support and belief in me although they may not understand my work presented here. And finally, I would like to dedicated this thesis to my husband, Qiuwen, for his love and patience in me.

Table of Contents

List of Figures

List of Tables

Chapter 1

Introduction

A commonly used method of increasing the output power of lasers is by combining the output of a number of lasers to form a laser array[1-4]. If a mechanism is provided so that a time-independent fixed phase relation is established in the electric field of the individual elements, the output beam is spatially coherent, resulting a far-field power density that is proportional to the square of the number of elements.

There are a number of techniques of initiating phase locking in a laser array. The most commonly used method is the evanescent coupling. In this scheme, a number of laser elements are placed in close proximity to one another so that a small amount of field coupling exists between the nearest neighbors. One- and two-dimensional phase-locked semiconductor laser arrays containing a large number of elements have been demonstrated[5-7]. The evanescent-coupled array geometry has also been used for producing high powers in Nd:YAG and CO_2 lasers. Other coupling methods include diffraction coupling and optical feedback from a common external cavity[3,8,9].

Earlier studies of semiconductor phased arrays were mainly focused on their spatial modal structures under the steady-state operating condition and on techniques to ensure the operation in the fundamental mode. The application of the coupled-mode theory to the evanescent-coupled waveguide system has led to the description of spatial eigenmodes of the coupled system, known as the supermodes. The predicted spatial profiles of the supermodes have been observed and well understood[10-13]. According to the supermode theory, an N-element evanescent-coupled laser array has N supermodes, each being the linear superposition of the eigenmodes of the individual elements. The lowest-order supermode is characterized by adjacent elements operating in the same phase, so that the far field pattern has a Gaussian-like pattern with a small beam divergence. The highest-order supermodes is characterized by adjacent elements having a phase difference of π, or out-of-phase, so that the far-field pattern has a dark fringe at the center. In semiconductor laser arrays, the out-of-phase mode has the largest modal gain. As a result, the array operates in the out-of-phase mode unless a modal selection mechanism is introduced. Various techniques for ensuring the in-phase mode operation have been studied. Nonetheless, little study has been done about the temporal behavior of such phase-locked laser arrays. Only until recently, have there been a few theoretical papers addressing the dynamical property of the phase-locked laser array[14-19].

These analyses, mostly numerical simulation, were based on the time-dependent coupled-mode theory. According to this theory, the phase-locking laser arrays were treated as coupled oscillators. Phase synchronization among the oscillators is reached through a self-organization process. A group of lasers with arbitrary initial phases can achieve phase locking through injection locking of evanescent waves. It was also predicted that phase synchronization is not always possible. For an N-element laser array coupled through any one of the means, there are 3N coupled dynamical equations of field amplitudes, phases, and population inversions[16,17]. For a ten-element laser array, there are 30 variables! Clearly, the dynamics in such system is very complex and rich in phenomenology. The numerical simulation has led to the conclusion that the laser arrays are intrinsically unstable and can develop irregular temporal behaviors such as self-sustained pulsations and chaos. The theory predicts that the period of the pulsation and the time scale of phase locking are inversely proportional to the coupling strength between the array elements[16,17]. Indeed, the predicted irregular behavior appears to have some experimental support. For example, the streak camera measurement of the time series of phase-locked semiconductor laser arrays revealed the existence of a sustained spiking phenomenon in the output of individual elements.[20] These spikes, 100-200 ps in duration at a repetition period of 300-400 ps, resembled the patterns predicted by some numerical simulations[20]. However, the predicted time scale of phase locking is much longer than the experimental observation. According to coupled-oscillator model, the time constant is on the order of 10 ns before the phase-locked state can be fully established in semiconductor laser arrays[17]. In contrast, the experimentally observed time constant of phase locking is less than 100 ps[19], which is three orders of magnitude smaller than the theoretical prediction. Despite the extensive numerical simulations, few systematic experimental studies has been done to verify the predicted temporal behavior. This is because the semiconductor laser arrays used in the experimental study contain 10 elements or 30 dynamical variables for the field amplitude, phase, and population inversion. The complexity of the system makes it difficult to relate the observed phenomena to the theoretical parameters.

Another important question that has not yet been addressed is the inter-element separation and the frequency detuning over which two laser elements can remain phase locked through the evanescent waves. In the past, the separation between adjacent elements of phase-locked semiconductor laser arrays is empirically chosen to be about 10 μm for gain-guided lasers and about 5 μm for index-guided lasers[21,22]. To the extent that phase locking can be viewed as injection locking through the evanescent waves, the maximum lateral distance for phase locking is presumably determined by the requirement that the injected field be larger than the field of spontaneous emission in the individual elements. Other factors such as the cavity Q-value, and the frequency detuning of individual elements can also affect the phase locking. The issue of tolerance of detuning is of interest because, there are frequency differences among the elements due to inevitable variations in cavity length and temperature.

These discrepancies and questions have prompted us to study phase locking in a simple laser array with well-controlled parameters. A two-element laser array is the simplest array with the least number of dynamical variables, namely, six. The requirement that the phase difference between adjacent elements is time independent further reduces the number of independent variables to five.

In general, there are three time constants (or scales) involved in the phase-locking process of a laser array. One is the phase-locking time, which we would like to determine. The other two are intrinsic to the type of lasers involved, namely, the upper level decay time and the photon lifetime. Of course, there is another time scale which is the delay feedback time in a system involving an external cavity. In order to reduce the complexity of the problem, and to bring about the essence of phase locking, we conduct the study in evanescent-coupled laser array which does not involve delayed feedback. Furthermore, in order to avoid any two of the three time scales to have the same order of magnitude, so to avoid any confusion as to which time scale, thus which dynamical variable, maybe dominant for the phase-locking process, we would like to "slow down" substantially the upper level decay time. Thus, a laser array with much slower upper level decay time can be chosen. Many solid-state and gas lasers are good candidates. It has become clear that miniaturized diode-pumped solid-state lasers are good choices for studying phase locking. Moreover, it was indicated by the coupled-mode modeling that while semiconductor laser arrays demonstrate stable phase-locked operation only over a small range of operating parameters[17] due to the strong amplitude-phase coupling and accompanied instability, solid-state laser arrays may exhibit stable phase-locking over a much wider range of coupling and operating parameters. Therefore it is of great interest to examine, both experimentally and theoretically, the coherence and phase dynamics of two-element evanescent-coupled solid-state laser arrays.

We have made experimental study of phase locking in a two-element evanescent-wave-coupled Nd:YAG laser array. It is important to note the similarities and differences between solid-state lasers and semiconductor lasers. For both of them, the polarization dynamics may be adiabatically eliminated when continuous wave (CW) operation is considered. Thus the lasers are well described by coupled rate equations for the complex field and population inversion. In both cases, the decay rate of photons in the cavity, $\gamma_c = \frac{c}{n}\left[\frac{1}{L} ln\, R^{-1} + a\right]$, where c is the speed of light in vacuum, n is the refractive index of the media, L is the cavity length, R is the effective reflectivity of end mirrors, and α is the internal loss, is larger than the decay rate of the population inversion $\gamma_{\parallel}$. For Nd:YAG lasers $\gamma_c = 10^6$ s^{-1} and $\gamma_{\|} = 4\times10^3$ s^{-1}, respectively, while for a semiconductor lasers, the corresponding values are $\gamma_c = 10^{12}$ s^{-1} and $\gamma_{\|} = 10^9$ s^{-1}, respectively. This means that while solid-state laser dynamics may be studied with conventional detectors, streak cameras are often necessary for studies of semiconductor laser arrays dynamics. For the present study we have simply used avalanche photo-diodes and a video camera system. Another important distinction between solid-state and semiconductor laser media is the large value of the "linewidth enhancement factor", α, for semiconductors (α=3-5) compared with $\alpha \approx 0$ for solid-state lasers. The α factor originates from the changes in real part of refractive index in semiconductors accompanying changes in the imaginary part. The nonzero α factor is a source of optical instability in semiconductor lasers because the field amplitude fluctuation is accompanied by frequency fluctuation which, through field coupling, leads to further field amplitude fluctuation. We will discuss this issue in greater detail later. Another novelty in our experimental technique is that the two-element laser array is photo-pumped by two semiconductor lasers. Technically, with photo-pumping, the separation between the elements can be continuously varied by adjusting the positions of the pumping beams. This enables us to investigate the dynamics of the array for a wide range of the coupling strength. In our experimental study, the two-element laser array is created in a Nd:YAG etalon by photo-pumping. The use of a monolithic cavity eliminates the need of optical alignment and greatly improves the stability and reproducibility. By introducing a small wedge angle in the etalon, a small and controllable frequency detuning between the two elements can be created for studying its effect on the locking range. Furthermore, diode-pumping also enables us to momentarily interrupt one or both elements and to record the time series of the phase recovery process.

This thesis is arranged as follows: in section II we will briefly review the theoretical foundations of laser arrays, including the supermode theory, the time-dependent coupled-mode theory, and prediction of laser instability based on the coupled-oscillator model. Section III describes our experimental setup and experimental results. In section IV we will summarize and discuss the discrepancies between the experimental results and previous theoretical predictions based on coupled-mode model. Also we present numerical modeling for the laser. The simulated patterns are compared with the measured mode profile. The experimentally determined boundary of phase-locking has been compared with the result calculated by a simple model based on mode competition theory. In section V, we analyzed the modal behavior in a gain-guided two-element semiconductor laser array. And finally in our last section, we conclude the important implication from our new understanding of the dynamics of laser array.

Chapter 2

Background

2.1 Laser array

Diode laser arrays have been widely used for applications that require high power or high brightness. The development of mirror damage limits the power density of a single-element semiconductor laser to about 1 MW/cm^2. Methods for increasing the power output have been to either enlarge the light emitting area using a single "broad-area" lasers or to fabricate several narrow-stripe diode lasers closely spaced on a common substrate so that they operate at a constant relative phase. The first phased array radiators at optical wavelength was reported in 1979 by Scifres et al[5]. A typical laser array, shown in Figure 1, consists of ten narrow-stripe lasers with a center spacing of 10 μm. Phase synchronization is achieved through the overlapping of evanescent waves with the nearest neighbors. Today, 1-D and 2-D diode laser arrays offering extremely high power levels have been used in applications such as illumination, solid-state laser pumping, and harmonic generation. In the meantime, theoretical models have been developed to analyze the experimental phenomena. Scifres et al. were the first to analyze the behavior of phase-locked arrays using so-called "simple diffraction theory"[10]. The modal patterns of a phase-locked laser array were treated as the interference fringes of a multiple slit. Butler et al. have reported the first coupled-mode analysis for an array of N coupled, identical elements[23]. They found that an array of N emitters has N normal modes or eigenmodes,

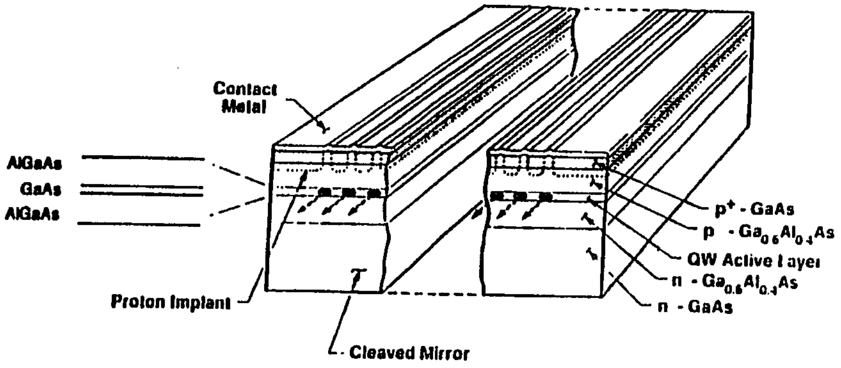

Figure 1 Schematic of a coupled multiple stripe laser.

which they chose to call array modes or supermodes. Shortly after, other research groups published independent work on coupled-mode formalisms applied to laser arrays[24,25].

2.2 Supermode theory

The optical characteristics, such as the near- and far-field intensity distribution of the eigenmodes, of a laser array can be understood in terms of the supermodes[24], i.e., the eigenmodes of the composite array waveguide. Consider an array of N coupled waveguide lasers as shown in Figure 2. The electric field of the array can be written as

$$E_y(x,y,z)=\sum_{l=1}^{N}\varepsilon_l(x,y)A_l(z)exp(i\beta_l z) \tag{1}$$

where $\varepsilon_l(x,y)exp(i\beta_l z)$, $l=1,2\cdots N$ is the single, transverse electric field, spatial mode of each individual laser waveguide when isolated from its neighbors, β_l is the complex propagation constant of each individual element, $A_l(z)$ is the z dependent amplitude due to the interaction among the array elements. Assuming that the coupling exists between the nearest neighbors, the coupled-mode equation for one element of the N-channel array can be written in the form

$$\frac{dE_i}{dz}=i\beta_i E_i+ik_{i,i+1}E_{i+1}+ik_{i,i-1}E_{i-1},\ i=1,2\cdots N \tag{2}$$

where k_{ij} is the coupling coefficient between the nearest neighbors. The set of equations can be combined into the matrix form as

$$\frac{d\vec{E}}{dz}=iM\vec{E} \tag{3}$$

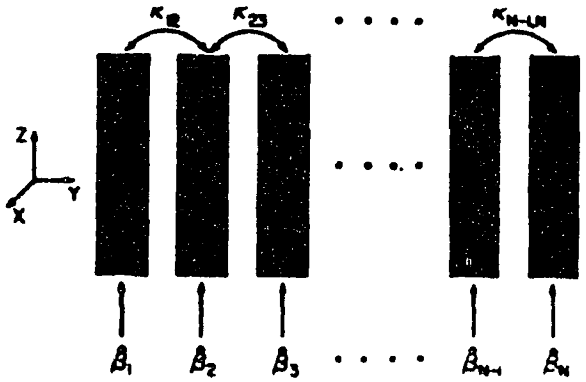

Figure 2 Schematic illustration of an N-channel laser array with coupling between nearest neighbors. After Kapon et al., Opt. Lett., Vol 10, 125 (1984)

where $\hat{E}$ is a vector whose elements are $E_l = A_l\, exp(i\beta_l z)$ and the only nonvanishing elements of the matrix M are $M_{l,l} = \beta_l$, with $l = 1,2\cdots N$ and $M_{l,l+1} = k_{l,l+1}$, $M_{l+1,l} = k_{l+1,l}$, with $l = 1,2\cdots N-1$.

The supermodes of the array are, by definition, the eigensolution of Eq (3), i.e., those vectors that satisfy

$$E^{\nu}(z) = E^{\nu}(0)exp(i\beta_{\nu}z) \tag{4}$$

where β_{ν} is the propagation constant of the vth supermode. Substitution of Eq. (4) into Eq. (3) gives

$$(M-\beta_{\nu}I)E^{\nu} = 0 \tag{5}$$

where I is the unit matrix.

Solution of Eq. (5) yields the N eigenvalues β_{ν} and the N supermodes E^{ν}, $\nu = 1,2\cdots N$. Each such eigenmode consists of a unique phase-locked combination of the individual channel amplitudes E_l^{ν} with a propagation constant β_{ν}.

The eigenvalues of a given N-channel array can be found by solving Eq (5) numerically. In the special case of identical channels with identical coupling coefficient $k_l = k$, $\beta_l = \beta$, the solution is

$$E_l^{\nu} = sin(l\frac{\pi\nu}{N+1}), \quad l = 1,2\cdots N \tag{6}$$

$$\beta_{\nu} = \beta + 2k\,cos(l\frac{\pi\nu}{N+1}), \quad l = 1,2\cdots N \tag{7}$$

The splitting between the propagation vectors of adjacent modes is on the order of $\frac{k}{N}$.

From (1) and (4), we can write the near field of the νth supermodes as

$$E^{\nu}(x,y,z)=\sum_{l=1}^{N}A_l^{\nu}\varepsilon_l(x,y)e^{(i\beta_{\nu}z)} \tag{8}$$

The field distribution in the far field, in the case of identical individual elements, is the Fourier transform of (8).

$$F^{\nu}(\theta)=E_0(\theta)\sum_{l=0}^{N-1}A_l^{\nu}e^{ik_0 l s\sin\theta} \tag{9}$$

where $E_0(\theta)$ is the pattern of a single element, s is the separation between adjacent elements and θ is measured from the normal to the exit plane.

Figure 3 shows schematically the near-field and far-field patterns of the supermodes in a five-element array when the coupling coefficient is uniform.[24]

A special case of interest is the two-element laser array. The eigenvectors have the form

$$\begin{aligned} E_1(z)&=\begin{vmatrix}-1\\1\end{vmatrix}e^{-i(\beta_0-|k|)z}\\ E_2(z)&=\begin{vmatrix}1\\1\end{vmatrix}e^{-i(\beta_0+|k|)z} \end{aligned} \tag{10}$$

$E_1(z)$ is thus the anti-symmetric mode, whereas $E_2(z)$ is the symmetric mode. The modal patterns are depicted in Figure 4.

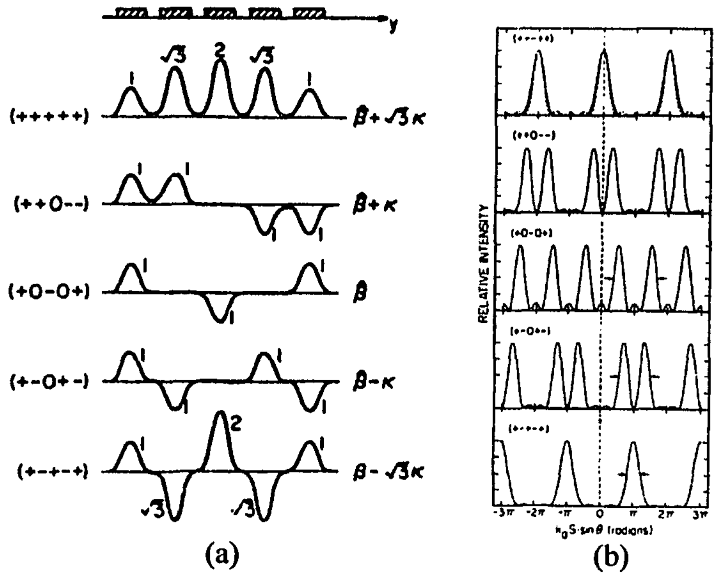

Figure 3 Schematic illustration of supermodes in a five-element array and uniform coupling. (a) near-field and (b) far-field
After Kapon et al., Opt. Lett., Vol 10, 125 (1984)

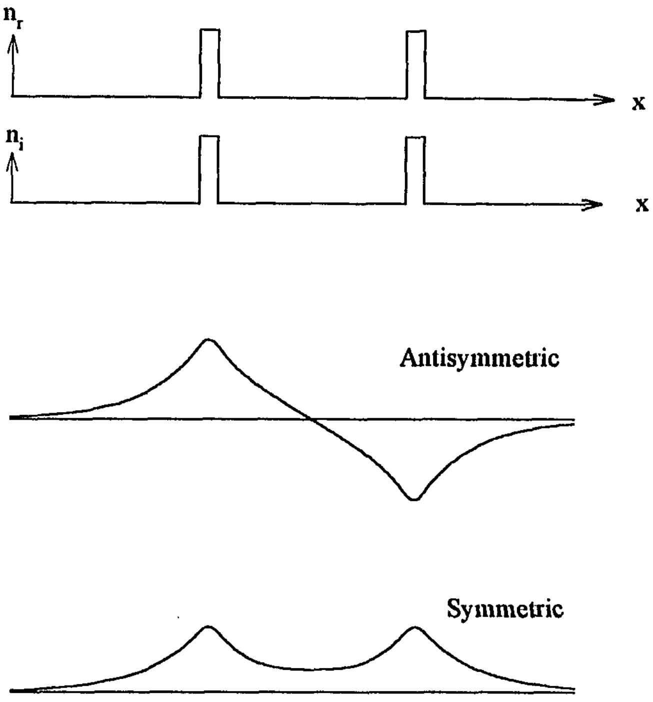

Figure 4 The transverse (x) modal field distribute of the supermodes of a two-element laser array whose real and imaginary parts of the refractive profile are shown at the top.

It is observed experimentally that semiconductor laser arrays tend to operate in the antisymmetric mode. This is because the antisymmetric mode has the largest modal gain due to the larger overlapping factor with the gain medium. Since the optical field goes through a null between the elements, the antisymmetric-mode also experience smaller absorption loss in the unpumped region. Unless a modal selection mechanism is built into the cavity, the array normally operates in the antisymmetric mode whose far-field has a dark fringe at the center.

2.3 Time-dependent coupled-mode theory

Recently, the temporal behavior and stability in laser arrays, especially in semiconductor laser arrays, have been modeled using the time-dependent coupled-mode theory which is essentially the coupled-mode theory in the time domain.

Spatial-dependent coupled-mode model has been widely used to analyze the passive waveguide arrays. In particular, modeling a passive structure using the coupled-mode analysis can predict a splitting of the propagation constant, leading to a determination of the eigenmodes of the composite structure. To model an active structure, such as a laser, both the gain and the refractive index distributions which affect the array mode characteristics must be included. The coupling leads to splittings in both the frequency, and the modal gain of the array modes. The gain splitting is important because it determines which of the supermodes can oscillate. The time-dependent coupled-mode theory has been used to analyze the dynamics of two resonators coupled through a common end mirror, injection locking, as well as directional-coupled guided waves. However the validity in applying the time-dependent coupled-mode model to laser arrays, in which the eigenmode of the composite waveguide has different resonant frequency from that of individual waveguide, has never been tested experimentally.

In the following we will describe the time-dependent coupled-mode theory, its basic assumptions, mathematical equations, and predictions based on numerical simulations.

We will consider a laser array consisting of two identical emitters placed side-by-side and coupled through the evanescent waves. The isolated emitter is assumed to support only the TE_{00} mode. We use a complete set of rate equations to describe the system. This analysis is based on the semiclassical laser theory modified to include terms that describe evanescent-wave coupling between adjacent elements of the array. We start from the rate equations of the electric field of the first element by adding the electric field from the second one. The equation can be written as:

$$\begin{aligned} \frac{d}{dt}[E_1(t)e^{i(\Omega_1 t+\phi_1(t))}] = \{i\omega_1 + \frac{1}{2}g'(1-i\alpha)(N_1 - N_{th})\}E_1(t)e^{i(\Omega_1 t+\phi_1(t))} + \\ i\kappa E_2(t)e^{i(\Omega_2 t+\phi_2(t))} \end{aligned} \qquad (11)$$

where N_i is the population inversion, E_i is the field amplitude of the individual lasers, and Ω_i and ϕ_i are the frequency and phase of the electric field, g' is the differential gain, $\kappa = \frac{\eta n}{c\tau_p}$ is the coupling coefficient , N_{th} is the threshold population inversion, α is the line width enhancement factor. Here the coupling coefficient is complex, the real part being related to the splitting of the frequency of the modes and the imaginary part being proportional to the splitting of the modal gains of the array modes. Following Ref[26], the coupled-mode theory can be used to calculate coupling strength η, as shown in Figure 5.

$$\kappa_{\substack{ab\\ba}} = \frac{\omega\varepsilon_0}{4}\int_{-\infty}^{\infty}[n_c^2(x) - n_{\substack{b\\a}}^2(x)]\varepsilon_y^{(a)}\varepsilon_y^{(b)}dx \tag{12}$$

where the transverse function $\varepsilon_y(x)$ is taken as

$$\varepsilon_y = \begin{cases} C\,exp(-qx) \\ C[cos(hx) - (q/h)\,sin(hx)] \\ C[cos(ht) + (q/h)\,sin(ht)]\,exp[p(x+t)] \end{cases} \tag{13}$$

and

$$\begin{aligned} h &= (n_2^2k^2 - \beta^2)^{1/2} \\ q &= (\beta^2 - n_1^2k^2)^{1/2} \\ p &= (\beta^2 - n_3^2k^2)^{1/2} \\ k &\equiv \omega / c \end{aligned} \tag{14}$$

The normalization condition gives

$$C = 2h\left[\frac{\omega\mu}{\beta(t + \frac{1}{q} + \frac{1}{p})(h^2 + q^2)}\right]^{1/2} \tag{15}$$

Separating the real and the imaginary part in Eq (11), we obtain two equations on the magnitude and phase of the electric field, respectively.

$$\begin{aligned} \frac{dE_1}{dt} &= \frac{1}{2}g'(N_1 - N_{th})E_1 + \frac{\kappa_r c}{n}[E_2\,sin(\Delta\omega t + \Delta\phi)] - \frac{\kappa_i c}{n}[E_2\,cos(\Delta\omega t + \Delta\phi)] \\ \frac{d\phi_1}{dt} &= \frac{\kappa_r c}{n}\frac{E_2}{E_1}cos(\Delta\omega t + \Delta\phi) + \frac{\kappa_i c}{n}\frac{E_2}{E_1}sin(\Delta\omega t + \Delta\phi) - \frac{\alpha g'}{2}(N_1 - N_{th}) \end{aligned} \tag{16}$$

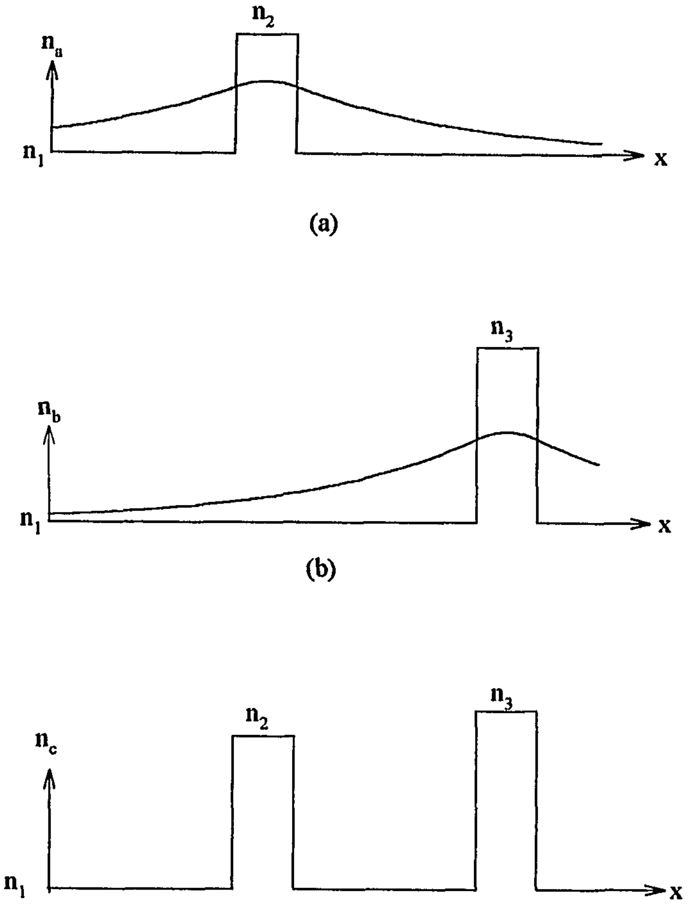

(a)

(b)

(c)

Figure 5 Spatial variation of refractive index for uncoupled waveguides $n_a(x)$ and $n_b(x)$ and for a coupled waveguide $n_c(x)$.

where $\Delta\omega=\Omega_1-\Omega_2$, $\Delta\phi=\phi_1-\phi_2$, and in YAG lasers, we assume $\Omega_i\approx\omega_i$. A usual form of rate equation has been adopted for population inversion, which can be expressed, assuming appropriated normalization for field amplitude E, as

$$\frac{dN_1}{dt}=P-\frac{N_1}{\tau_s}-[\frac{1}{\tau_p}+g'(N_1-N_{th})]E_1^2 \tag{17}$$

where τ_s is the lifetime of the excited state, τ_p is the photon lifetime, and P is the pumping rate. The equations for the second element are identical to those of the first one. With proper variable replacement, the complete set of coupled-mode equations for a two-element laser array are:

$$\frac{dE_1}{dt}=\frac{g_1'}{2}(N_1-N_{th})E_1+\frac{\kappa_R c}{n}[E_2\sin(\Delta\phi)]-\frac{\kappa_I c}{n}[E_2\cos(\Delta\phi)] \tag{18}$$

$$\frac{dE_2}{dt}=\frac{g_2'}{2}(N_2-N_{th})E_2-\frac{\kappa_R c}{n}[E_1\sin(\Delta\phi)]-\frac{\kappa_I c}{n}[E_1\cos(\Delta\phi)] \tag{19}$$

$$\begin{aligned}\frac{d(\Delta\phi)}{dt}&=-\frac{\alpha g'}{2}(N_2-N_1)+\Delta\omega+\frac{\kappa_R c}{n}[\frac{E_2}{E_1}-\frac{E_1}{E_2}]\cos(\Delta\phi)\\&\quad+\frac{\kappa_I c}{n}[\frac{E_2}{E_1}+\frac{E_1}{E_2}]\sin(\Delta\phi)\end{aligned} \tag{20}$$

$$\frac{dN_1}{dt}=P-\frac{N_1}{\tau_s}-[\frac{1}{\tau_p}+g_1'(N_1-N_{th})]E_1^2 \tag{21}$$

$$\frac{dN_2}{dt}=P-\frac{N_2}{\tau_s}-[\frac{1}{\tau_p}+g_2'(N_2-N_{th})]E_2^2 \tag{22}$$

The linewidth enhancement factor α, defined as the ratio of the changes in the real part of the refractive index to the imaginary part of the refractive index with changing population inversion, represents the amplitude-to-phase coupling in a laser. In a laser with nonzero α, any change in the amplitude of the laser is accompanied by a shift in laser frequency. Through interference effect, the shift in laser frequency leads to further changes in the amplitude, resulting in complicated dynamics. In semiconductor lasers, α ranges from 1-5. For solid-state lasers, α can be considered as zero.

This set of equations contains five independent variables. The time series of the field amplitude and relative phase can be obtained by direct integration of Eq (18)-(22). In general, in a N-element system, the time-dependent coupled-mode equations become

$$\begin{aligned}\frac{dE_i}{dt} &= \frac{g'}{2}(N_i - N_{th})E_i + \frac{\kappa_R c}{n}\left[E_{i+1}\,sin(\Delta\omega_i t + \Delta\phi_i) - E_{i-1}\,sin(\Delta\omega_{i-1}t + \Delta\phi_{i-1})\right] \\ &\quad - \frac{\kappa_I c}{n}[E_{i+1}\,cos(\Delta\omega_i t + \Delta\phi_i) + E_{i-1}\,cos(\Delta\omega_{i-1}t + \Delta\phi_{i-1})]\end{aligned} \tag{23}$$

$$\begin{aligned}\frac{d\phi_i}{dt} &= -\frac{\alpha g'}{2}(N_i - N_{th}) + \frac{\kappa_R c}{n}\left[\frac{E_{i+1}}{E_i}cos(\Delta\omega_i t + \Delta\phi_i) + \frac{E_{i-1}}{E_i}cos(\Delta\omega_{i-1}t + \Delta\phi_{i-1}\right] \\ &\quad - \frac{\kappa_I c}{n}\left[\frac{E_{i+1}}{E_i}sin(\Delta\omega_i t + \Delta\phi_i) - \frac{E_{i-1}}{E_i}sin(\Delta\omega_{i-1}t + \Delta\phi_{i-1}\right]\end{aligned} \tag{24}$$

$$\frac{dN_i}{dt} = P - \frac{N_i}{\tau_s} - (\frac{1}{\tau_p} + g'(N_i - N_{th}))E_i^2 \tag{25}$$

where $\Delta\omega_i = \omega_i - \omega_{i+1}$, $\Delta\phi_i = \phi_i - \phi_{i+1}$

Through numerical integration, it has been predicted that a laser array is intrinsically unstable and phase synchronization is not always be reached. When phase synchronization fails, the time series of the amplitude and phase can exhibit a variety of dynamics, including sustained regular pulsation and irregular pulsation, and even chaos.

Previous numerical modeling predicts that laser array is dynamically unstable in three cases[14,16,17,27]

(a) $N>2$ or

(b) $N\geq 2$ and $\alpha\neq 0$, or

(c) $N=2$ and $\Delta\omega\neq 0$

The instability of case (a) is a result of increased dimension in a nonlinear system. An example of the calculated irregular time-series of the field amplitudes and phase of the individual elements is shown in Figure 6 for a five-element array. The presented instability can be regarded as self-induced phase turbulence because the intensity fluctuation of individual emitters is negligibly small while the chaotic evolution of relative phases persists. This inherent dynamics was attributed to the destruction of phase locking of multiple emitters due to population dynamics.

Case (b) applies to semiconductor lasers in which the amplitude-phase coupling is large and the phase self-organization process is interrupted by the changing frequency of the individual elements during the interaction. The computed time-series of amplitude and relative phase of a two-element semiconductor laser array are shown in Figure 7 using the parameters of Ref 17. The relative phase is found to undergo sustained oscillation between $\pi/2$ and $-\pi/2$. The oscillating phase also leads to conclusion that beam scanning may be taking place in semiconductor laser arrays[27]. This prediction, first proposed by Ref 16,

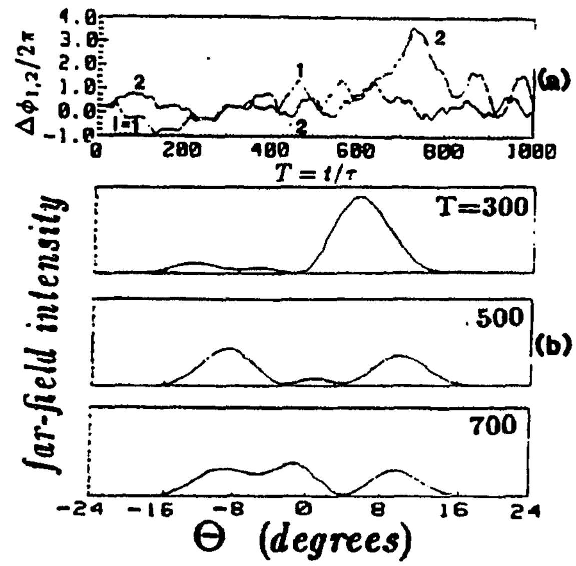

Figure 6 Calculated chaotic time series of (a) relative phase, and (b) time-dependent far-field patterns in a five-element coupled-waveguide laser.
After Otsuka, Phys. Rev. Lett., Vol 65, 329 (1990).

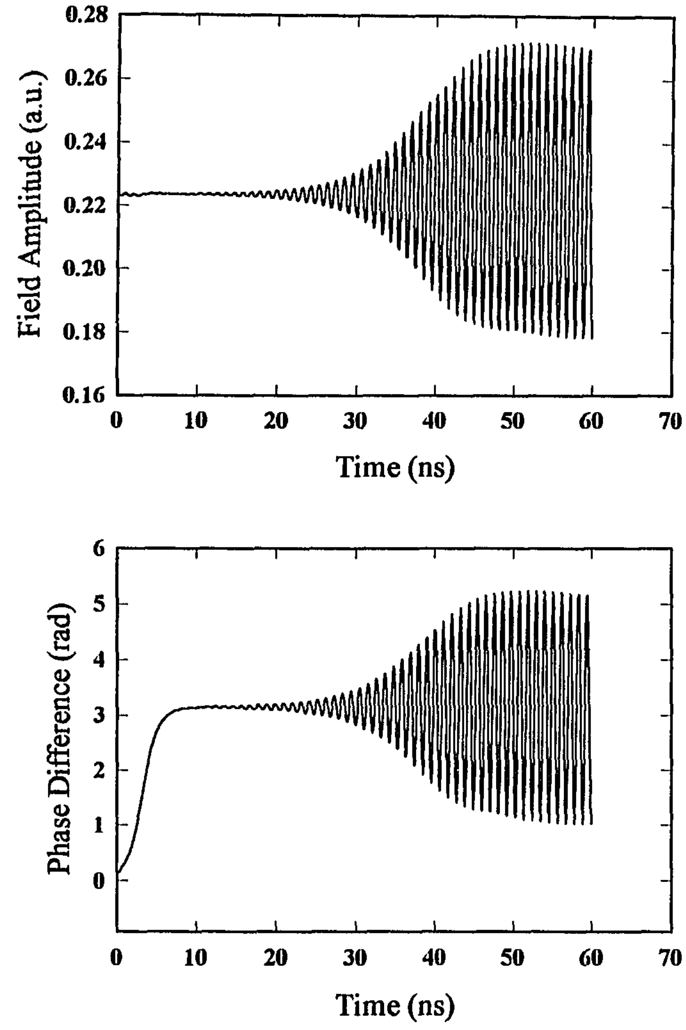

Figure 7 Calculated periodic oscillations in (a) field amplitude and (b) relative phase in a two-element semiconductor laser array in the unstable regime.

was the basis of the notion that semiconductor laser arrays are intrinsically unstable, the facinating laser dynamics motivated our research project.

Case (c) represents a realistic situation in all types of laser arrays in which the individual elements do not have the same resonance frequency due to variations in cavity length, temperature, and population inversion. An example of this type of optical instability is shown in Figure 8 for a two-element Nd:YAG laser array with a frequency detuning of 5 MHz.

So far, there has been no systematic experimental verification of the predicted instability in laser arrays. The only phenomenon that was widely cited as the evidence of instability was streak camera study of irregular pulsing behavior in a ten-element semiconductor laser array[20]. Briefly, the time series of the output intensity of one of the elements was found to exhibit irregular pulsations in the 100-ps time scale while the total output is relatively "quiet". This self-sustained pulsing behavior was attributed to the type (b) instability caused by amplitude-phase coupling. The numerical modeling based on the coupled rate equation seemed to support the existing of instability. However, it is also well-known that semiconductor laser arrays normally operate in multiple longitudinal mode. The sustained pulsing could also found explanation from the beating among the longitudinal modes. These questions can be answered only through a systematic study with well-controlled experimental conditions. The predicted instability in the amplitude of the lasing field can be detected from the intensity fluctuation of the laser output in the near field. The instability in the relative phase leads to beam scanning and can be detected from

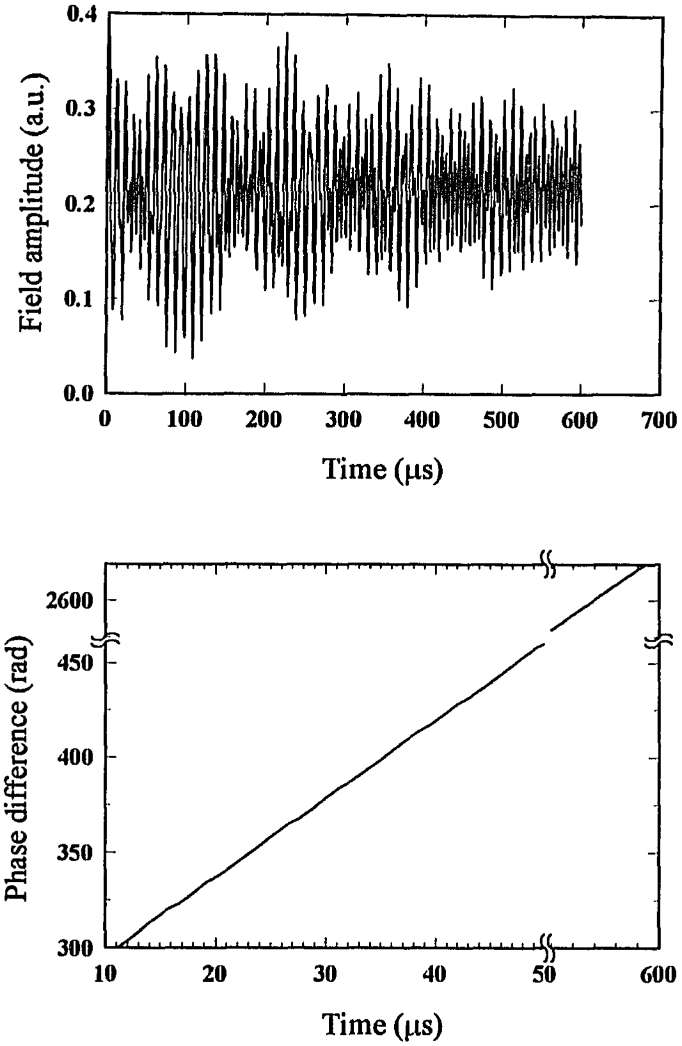

Figure 8 Calculated (a) irregular oscillation of electric field amplitude and (b) unbounded phase evolution in a two-element Nd:YAG laser array with frequency detuning of 5 MHz.

the intensity fluctuation in the far field. In the following sections, we will present an expriment designed to test these predictions.

Chapter 3

Experiment

3.1 Diode pumped Nd:YAG laser array

The experimental setup for studying the phase locking process of the evanescent-coupled lasers is shown in Figure 9 and 10. Two spatially-separated parallel lasing filaments are created by end-pumping a monolithic Nd:YAG etalon using two AlGaAs/GaAs quantum-well diode lasers. The two-element diode-pumped Nd:YAG laser array provides us with a simple and stable system to study the phase-locking. The diode lasers are temperature regulated to generate outputs at 809 nm, the wavelength of the absorption peak of the Nd^{3+} ions in the Nd:YAG crystal. For a cavity length of 5mm, approximately 98% of the pump energy is absorbed. The pumping beams from the quantum-well diode lasers are linearly polarized, with the polarization direction lies in the junction plane. The two beams are combined by a polarizing beam splitter, which transmits one polarization and reflects the orthogonal polarization. In order to combine the two beams without loss, a half-wave plate is placed in the path of one of the pumping beams to rotate the polarization of that beam by 90°. The light emitting area of the active layer of diode is 60 μm×1 μm. The asymmetry in the dimension makes the light emitted from diode highly asymmetric. The beam divergence angles in the vertical (Y) and horizontal (X) directions are 45° and 10° respectively. The pumping beams are focused on to the YAG crystal by two collimating lenses, one for each branch, with a focal length of 6.5

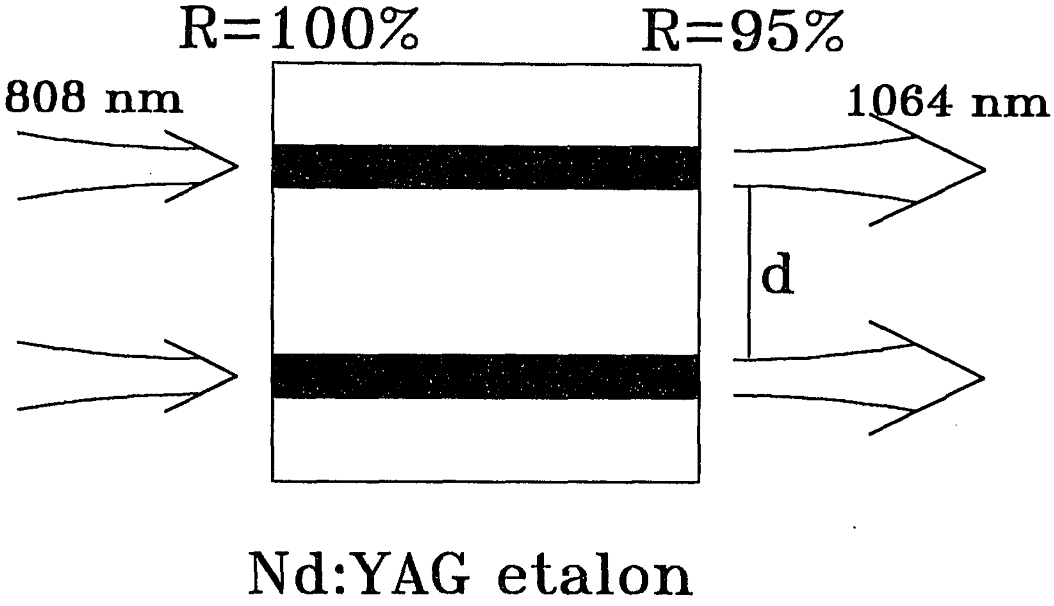

Figure 9 Schematic of diode-end-pumped two-element laser array in a Nd:YAG etalon

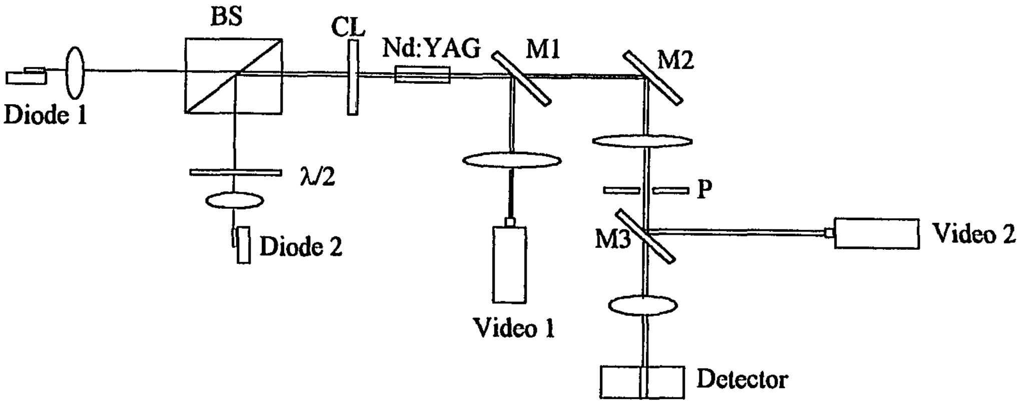

Figure 10 Schematic of experimental setup

mm, they are followed by a common cylindrical lens with a focal length of 2.5 cm. Each of the two collimating lenses is mounted on a 3-dimensional (3-D) translation stage, while the position of the diode lasers are fixed. The focusing in the X direction is determined by the common collimating lens while the focusing in the Y direction is determined by the individual focusing lenses. The position of cylindrical lens can be adjusted along the z direction to produce smallest spot at the center of the crystal. The pumping beams are quite uniform inside the crystal and expand by less than 8 μm in the y-direction throughout the crystal and by less than 600 μm in the x-direction. Fine tuning of the separation with an accuracy of 0.5 μm is achieved by displacing the laser diode using a piezoelectric transducer. Thus the coupling strength between the two laser elements in the array can be continuously varied without affecting the alignment by adjusting the position of one of the pumping beams.

The Nd:YAG crystal is 5-mm in length and 5-mm in diameter. The two end surfaces are polished flat and parallel to within 1 arcsecond. The end facing the pumping beams is coated for high reflectivity (R>99.9%) at 1064 nm and high transmission (T>90%) at 808 nm. The output end is coated for 95% reflectivity at 1064 nm. The crystal is mounted on an angular orientation stage. The lowest threshold pumping power for CW operation, 110 mw, is achieved when the axis of the crystal coincides with the propagation axis of the pumping beams. The residual wedge results in a slight difference in the individual operating frequencies of the two elements due to the small cavity length difference. This detuning frequency can be detected from the frequency of beat waves when the two elements are unlocked. The frequency detuning can be controlled by rotating the etalon about the axis of propagation.

Both the near- and far-field intensity distributions are monitored using two infrared video cameras. For the near-field observation, the magnified image of the intensity distribution of the array at the output mirror is projected onto one of the cameras. After calibration, the separation between the two waveguides can be measured directly from the screen of the video monitor. The diameter of the pumping beams is about 50 μm at the crystal.

For the far-field distribution observation, the detection setup is arranged as following: A small area avalanche Ge detector is used to detect the output light. In between the output mirror and the detector, two lenses and a pinhole are inserted. The beam is first expanded by a long focal length lens. And then a pinhole, mounting on a 3-D translation stage, is placed enroute to select the portion needed. Finally another lens is used to focus the light onto the detector. Also a small part of the beam is reflected into a second video camera after passing through the pinhole to be monitored.

3.2 Wave-guiding properties in Nd^{3+}:YAG laser array

The wave-guiding mechanism in the array is determined by the combination of the thermally-induced refractive-index change and gain-induced wave-guiding. In Nd:YAG the refractive index increases with respect to temperature is about 7×10^{-6}/K.[28] The real part of the refractive index step Δn_r, caused by the thermal effect, can be estimated experimentally using the following procedures. The magnitude of the thermally-induced refractive index step can be estimated by the frequency shift of the beat waves of two unlocked elements when the power of the pumping beam of one of the elements is varied. The power of pumping beam is controlled by the injection current of the semiconductor laser. For example, if the injection current of one of the semiconductor lasers is increased by δI, the beat frequency will change by δf correspondingly, due to the change of refractive index δn. Thus, by using $-\delta f/f=\delta n/n$, where $f=3\times10^{14}$Hz, n=1.8, we can relate the change of refractive index δn with the small change of the current δI. We have found that as one of the pumping current changes by 10 mA, the beat frequency changes by 8 MHz, corresponding to $\delta n=4.8\times10^{-8}$. To the extend that the temperature increase is proportional to the pumping current, the total change of refractive index would be 1×10^{-6} for a typical CW pumping current of 200 mA. Although the refractive-index profile of the waveguide is expected to be bell shaped, to simplify the analysis, we assume a rectangular profile with an index step of real 2×10^{-6} in height and 50 μm in width in the theoretical calculation. The calculated full-width-half-maxima (FWHM) of the eigenmode of the waveguide is about 150 μm. This calculated value is in close agreement with the experiment.

The imaginary part of the refractive index step can be estimated from the gain and loss of the cavity by:

$$\Delta n_i = \frac{g\lambda}{4\pi n_0} \tag{26}$$

where g is the gain coefficient in cm^{-1}, λ =1.06 μm is the wavelength of Nd:YAG laser in vacuum, and n_0 =1.8 is the refractive index of YAG, and Γ is the modal overlapping factor with the pumped gain medium. Because the reflectivity of the two mirrors are 95% and 100%, respectively, the round-trip loss is 5%. The imaginary part of the modal index at threshold is calculated to be about 4.8×10^{-7}. Taking into account the confinement factor of 27%, the imaginary part of the refractive index step is 2×10^{-6}. Although the real and imaginary part of the refractive index step are comparable, numerical calculation shows that the electric-field profile calculated with and without the imaginary part has only negligible difference. Thus this waveguide can be considered as index-guided. The real and imaginary parts of the refractive-index steps and the calculated modal profiles are shown in Figure 11. The parameters for Nd^{3+}:YAG used in the text are summarized in Table I. When the two elements are separated by a large distance, the coupling is weak and the two individual laser elements operate independently. For pumping area of 50 μm, the beam diameter is 190 μm in the near field and the beam divergence is 0.07 degree in the far field. The far-field pattern has a Gaussian-like pattern which is the incoherent addition of the intensity of the two elements. When the separation is less than 600 μm, phase locking is observed. At this point, the far-field pattern exhibits the typical two-lobed pattern with a dark fringe at the center, characteristic of the antisymmetric mode. This anti-symmetric mode is dominant because the overlap of the optical field with the lateral spatial gain distribution is maximized for this mode. The optical intensity goes through null between the two elements, so that the mode "avoided" the region of low optical gain. For example, for an inter-element of 300μm, the overlapping factor with gain region is $\Gamma=25\%$ for the symmetric mode and $\Gamma=31\%$ for the antisymmetric mode respectively.

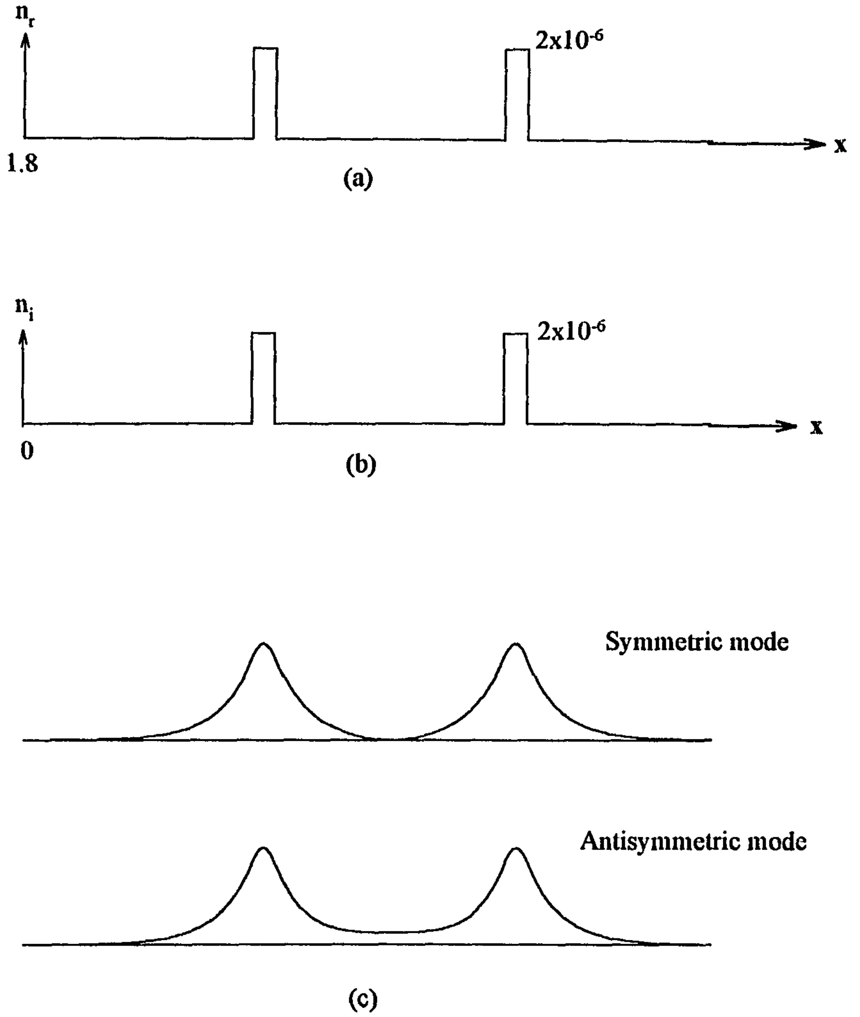

Figure 11 The refractive index profile of the (a) real part and (b) imaginary part of a two-element laser array and (c) computed modal profile.

Table I The parameters for Nd:YAG laser array

Parameters	Values
Cavity length	5 mm
Crystal diameter	5 mm
Coating	Input: HR@1064 nm & HT@809 nm Output: 95%@1064 nm
Pumping area	50 μm x 50 μm
Near-field	190 μm
Far-field divergence angle	0.07 degree
Change of n_r	$2\text{x}10^{-6}$
Change of n_i	$2\text{x}10^{-6}$

For separations less than 200 μm, the laser is found to operate in mixed symmetric and antisymmetric modes. The mixed mode operation is characterized by a reduced fringe contrast and a beating pattern at the frequency corresponding to the frequency difference of the two modes. Shown in Figure 12 are the photographs of the far-field of locked state (a) and unlocked state (b).

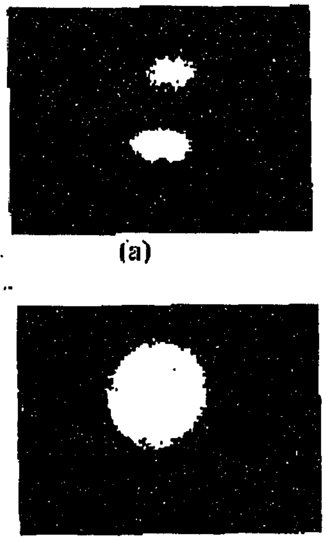

(a)

(b)

Figure 12 Photographs of the far-field patterns of (a) phase-locked state in the antisymmetric mode and (b) the unlocked state.

3.3 Temporal evolution of phase locked mode

One of the main objectives of this study is to observe the instability and transitional behavior of phase locking. We are interested to see if the relative phase of the two elements undergoes a time-dependent transition. The best way to monitor such transition is to carry out a measurement of the time series in the far-field. The far-field intensity at any given position can be approximated by $[E_1 + E_2 e^{i(\phi_0+\Delta\phi(t))}]^2$ where E_1 and E_2 are the field amplitudes of individual element, ϕ_0 is the relative phase at the steady state, and $\Delta\phi(t)$ is the time-dependent phase deviation from the steady state. Thus any transient relative phase oscillation about the steady-state values as predicted in Ref 17, would result in an intensity oscillation. Such intensity oscillation, if any, can be observed by placing a small area detector at the center of the far-field pattern.

In order to observe the dynamics of phase locking after the laser is turned on, the CW laser array is momentarily turned off for a short period and the recovery of phase locking is monitored by a photo-diode in the far-field. In our experiment, the pump beam can be turned off by superimposing a negative current pulse to the positive CW current of diode laser. The independent power supply provides a convenient way to interrupt one or both pumping beams. The turn-off period is about 250 ns which is short enough not to cause any heating effect or affect the waveguide and long enough to completely turn off the laser (the photon lifetime of our system is 1.2 ns). The laser operates in the fundamental transverse mode with CW pumping current slightly above the threshold.

When the laser is operating in the out-of-phase mode, we adjust the size of pinhole to select only the dark center and focus the light on to the fast detector. By moving the pinhole to the valley and peak of the far-field pattern, the time series of the intensity of the peak and valley are recorded. Figure 13 shows the time series of intensities measured at the peak and valley of the far-field distribution. If the phase locking is a slow evolutionary process, we would expect to see the oscillatory behavior in the time series as shown in Figure 14. However, we have found that when the laser is turned on, the intensity undergoes a damped relaxation oscillation and its damping time constant is comparable to that of the relaxation oscillation of the individual laser. Most importantly, the intensity at the center of the far-field pattern is zero as soon as the lasing begins and maintains throughout the process. This observation indicated that phase locking is developed as fast as the occurrence of first peak of the relaxation oscillation and the development of phase locking does not undergo a slow-evolutionary process as predicted by the coupled oscillator theory. Furthermore, once the coupling is strong enough to ensure phase locking, the time it takes for this fast locking process is found to be independent of the coupling strength. The fast locking is also independent of whether one or both elements are interrupted.

3.4 Detuning characteristics of laser arrays

The frequency detuning is the difference between the resonance frequencies of the oscillating modes of the individual elements. In general, the frequencies of the individual elements in the array when operated in the absence of the other are not exactly the same due to variations in the effective cavity length caused by variation in cavity length,

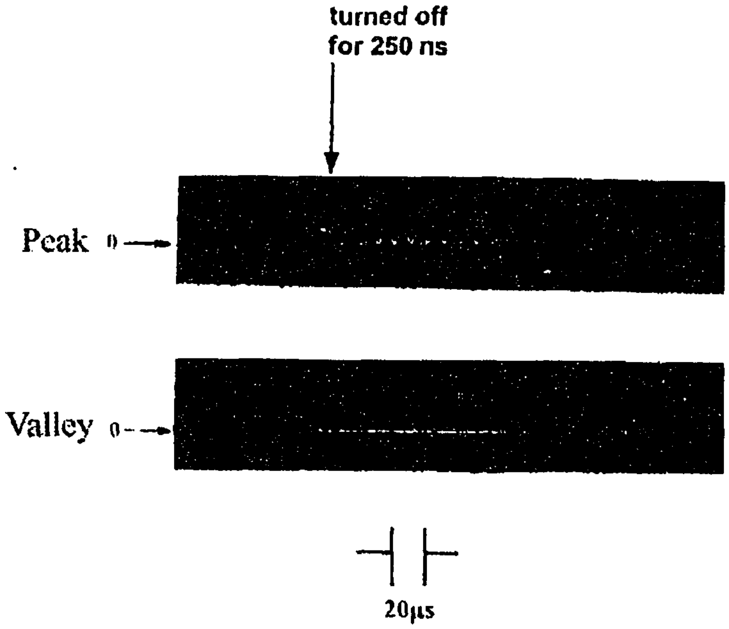

Figure 13 Time series of intensities measured at the peak (upper trace) and valley (lower trace) of the far-field distribution. The 250 ns turned-off period is not resolved in this time scale.

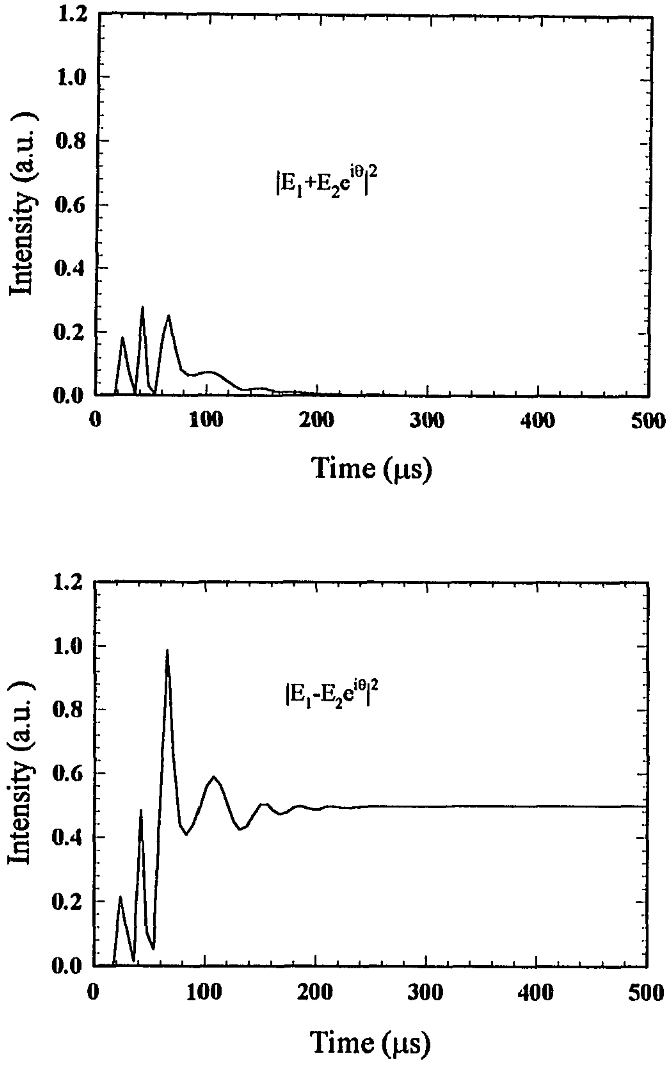

Figure 14 Time series of intensities at the valley (a) and peak (b) of the far-field intensities calculated using coupled-oscillator model.

temperature, cross-sectional area and population inversion. It is of interest to see how these elements with different frequencies become phase locked and to measure how large a detuning the system can tolerate when phase locking is maintained.

The experimental setup is similar to the one described in Figure 9, except that a 10-seconds wedge angle between the two-end mirror surfaces is deliberately introduced. The wedge results in a small difference in the round-trip optical path for the array elements and, therefore, a small difference in their individual operating frequencies. By rotating the Nd:YAG rod along the axis of the propagation, the detuning between the two elements can be "tuned" from the minimum to maximum for a fixed separation between the two elements. The difference in the oscillation frequency manifests itself as the beating waves when the two elements are unlocked. The beat wave can be detected by an avalanche photo-diode placed in the far field and its frequency can be measured using a Tektronix 7L13 spectrum analyzer. On the other hand, when the two elements are phase locked, the array operates in a single frequency without beat waves. Thus the occurrence of beat waves signifies the breaking of phase locking.

To generate the map of the boundary of phase locking, the two lasing elements are brought close to each other so that phase locking is established. At this point, the far field intensity distribution has a two-lobed profile with a dark fringe at the center. These two elements are then pulled away continuously until a beat note appears on the screen of the spectrum analyzer. The frequency of the beat waves, as they first appear, is considered as the maximum tolerance of the detuning for phase locking. At this point the corresponding separation between the elements is recorded. The procedure is then repeated for different wedge angles in the etalon. The detuning frequencies are then plotted as a function of the separations. The data are shown in Figure 15. The detuning frequency at which the transition takes place range from 200 MHz for d=300 μm to 2 MHz for d=600 μm. In our experiment the separation at 600 μm appears to be the maximum distance for phase locking. No phase-locked mode is observed for separations larger than 600 μm.

The modal patterns and the transitional behavior in the vicinity of the boundary is worth noting. For small inter-element separation and large detuning, the transition from the phase-locked to unlocked states is abrupt as the boundary is crossed along line A in Figure 15. As the boundary is crossed the occurrence of the beat wave is accompanied by a distinct change in the modal patterns from the two-lobed far-field profile, shown in Figure 16(a), to the single-lobed profile shown in Figure 16(b). For large inter-element separation and small detuning, the transition is gradual and the phenomenon is more complex. As the two elements are pulled away following path B (in Figure 15), the occurrence of the beat wave is accompanied by a gradual reduction of the contrast ratio in the two-lobed far-field pattern, as shown in Figure 17(b). As the separation is further increased, the patterns undergo an evolution from the two-lobed profile to the three-lobed profile with a peak at the center, as shown in Figure 17(c), and for further increase of separation, to the broad single-lobed profile as shown in Figure 17(d).

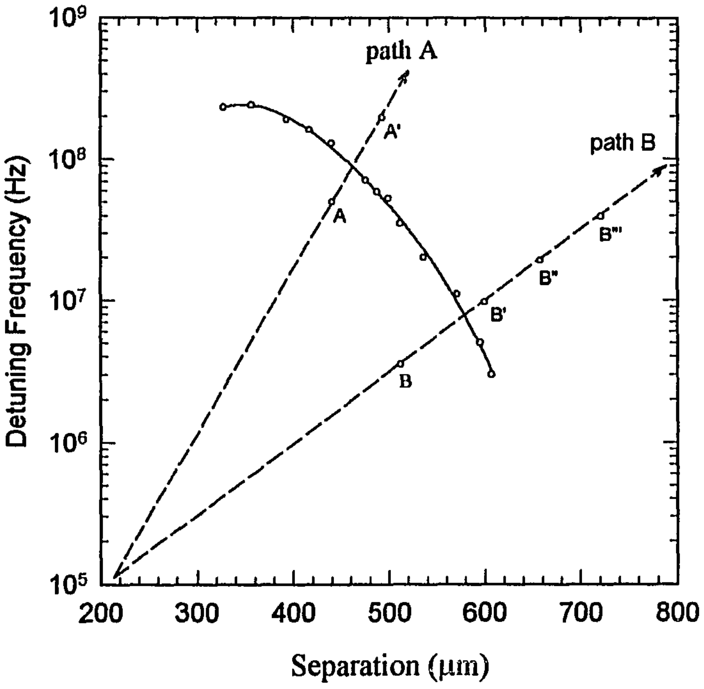

Figure 15 The boundary of phase locking in the space of detuning and separation. The closed circles are the experimental data.

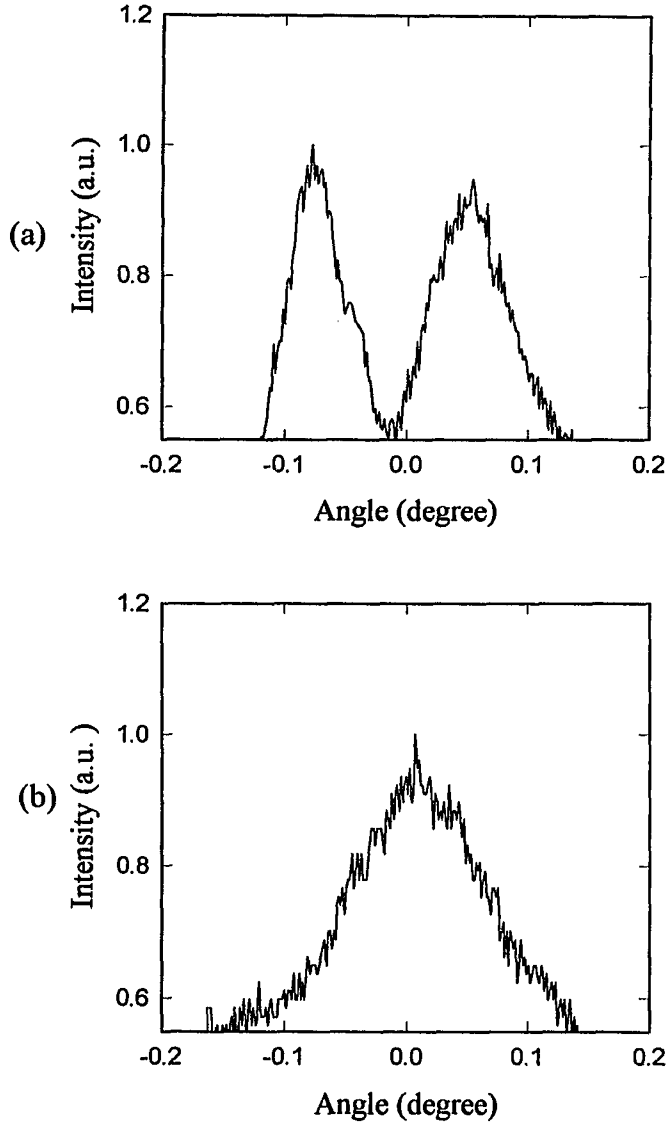

Figure 16 Observed far-field patterns at various positions along path A, (in Figure 15, measured at points (a) A and (b) A'.

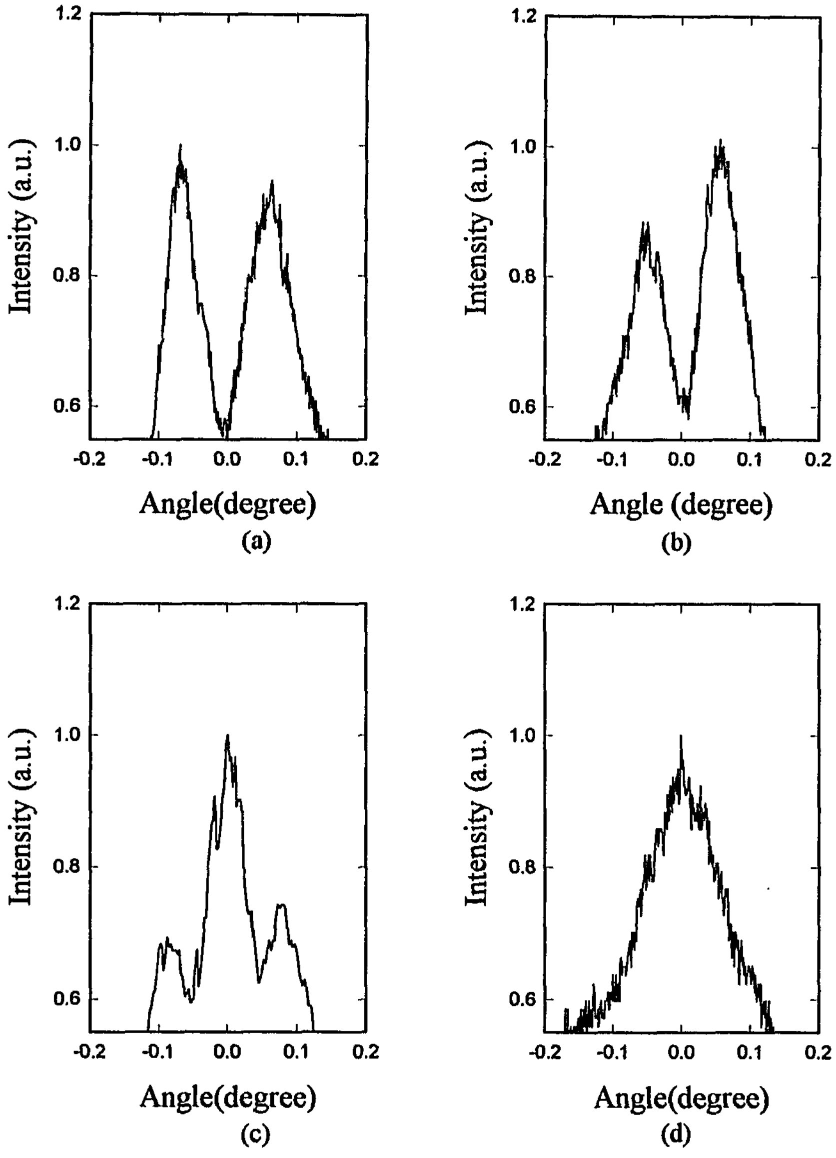

Figure 17 Observed far-field patterns at various positions along path B, (in Figure 15,) measured at positions (a) B, (b) B', (c) B'', (d) B'''.

Chapter 4

Analysis

4.1 Comparison with the predictions of coupled-oscillator model

At first, we attempted to model the array dynamics by treating the effect by a coupling term between electric fields of two identical lasers follow the equations (18)-(22). The parameters are:

τ_s=200 μs

$$\tau_p = \frac{n}{c(\alpha - 1/l\,ln\sqrt{R_1 R_2})}$$

where n is the refractive index of media, c is the speed of light in vaccum, $\alpha \approx 0$ is an average distributed loss constant per round-trip, R_1 and R_2 are the mirrors' reflectivity R_1R_2=0.95, and l =10 mm is the round-trip cavity length. τ_p calculated to be 1.2 ns. g' and N_{th} satisfies $g'N_{th}\tau_p$=1.

For convenience we introduce the following normalized variables and parameters:

$$\begin{aligned}
&X_i = (\frac{1}{2}g'\tau_s)^{1/2}E_i\\
&Z_i = (1/2)g'N_{th}\tau_p(N_i/N_{th} - 1)\\
&p = (1/2)g'N_{th}\tau_p(P/P_{th} - 1) \qquad (27)\\
&\eta = (\kappa c/n)\tau_p\\
&T = \tau_s/\tau_p
\end{aligned}$$

Then for a two-element array, the coupled-mode equations become

$$\frac{dx_1}{d\tau} = z_1 x_1 + \eta_R x_2 \sin\theta - \eta_I x_2 \cos\theta \tag{28}$$

$$\frac{dx_2}{d\tau} = z_2 x_2 - \eta_R x_1 \sin\theta - \eta_I x_1 \cos\theta \tag{29}$$

$$\frac{d\theta}{d\tau} = \Delta\omega + \eta_R\left(\frac{x_1}{x_2} - \frac{x_2}{x_1}\right)\cos\theta + \eta_I\left(\frac{x_2}{x_1} + \frac{x_1}{x_2}\right)\sin\theta \tag{30}$$

$$T\frac{dz_1}{d\tau} = p - z_1 - (1 + 2z_1)x_1^2 \tag{31}$$

$$T\frac{dz_2}{d\tau} = p - z_2 - (1 + 2z_2)x_2^2 \tag{32}$$

Following the spirit of Ref 15-16, we tried to use the above Eq. (19)-(23) with only real part of coupling coefficient to simulate the phase-locking process after the laser array is turned on. In Figure 14(a) and (b), we show the calculated $|E_1 + E_2 e^{i\theta}|^2$ and $|E_1 - E_2 e^{i\theta}|^2$, corresponding to the minimum and maximum intensities of the two-lobed far-field pattern. The time constant for the establishment of the phase-locked state is on the order of 300 μs. Also, the recovery process from below the threshold to the steady-state intensity has been simulated when one of the element is turned off for 250 ns, Figure 18. The perturbation is found to transmit from one element to the other and back, the time constant is η_R / τ_p. In the two-element the calculated time-constant is on the order of several μs.

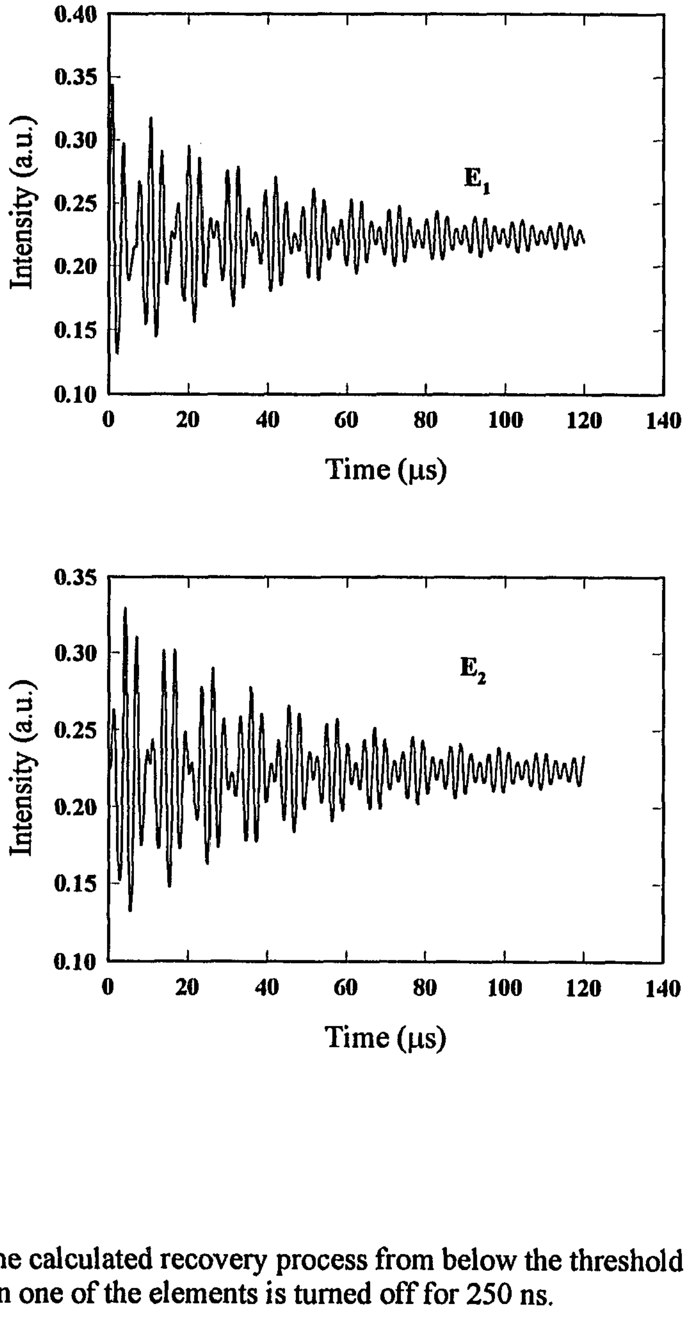

Figure 18 The calculated recovery process from below the threshold to the steady-state intensity when one of the elements is turned off for 250 ns.

The experimentally observed fast locking and lack of a slow evolutionary process and slow energy transfer between the elements are not consistent with previous prediction based on the coupled oscillator model. This discrepancy can be in part removed by introducing a large imaginary part of the coupling strength. The imaginary part of the coupling strength and its effect on phase locking time was not properly taking into account in most earlier literatures on the dynamics in laser arrays. We have found that even a small imaginary coupling strength can result in a fast locking that may explain the fast locking and lack of a slow evolutionary process. Figure 19 shows a calculated time series of the $|E_1+E_2e^{i0}|^2$ and $|E_1-E_2e^{i0}|^2$ evolution with $\eta_i \neq 0$, defined as

$$\eta_i = \frac{Im(n_{in-phase}) - Im(n_{out-of-phase})}{2\,Im(n_{single})}.$$

Based on the coupled-oscillator model, the phase-locking process is treated as an injection locking process. The tolerance of detuning and the locking range is determined by the coupling strength. The imaginary part of the coupling strength decreases nearly exponentially with the separation, shown in Figure 20. Thus we would expect a corresponding decrease in the tolerance of detuning as the separation increases. A numerical simulation is carried out to determine the tolerance of detuning for phase locking. The system is considered to be phase locked if, after periods of transient oscillations, the amplitude and the relative phase reach a steady state and the two elements operated in same frequency. The system is considered unlocked if the relative phase increases linearly with time, creating a beating phenomenon of two independently operated lasers. The locking range and locking dynamics are strongly influenced by the magnitude

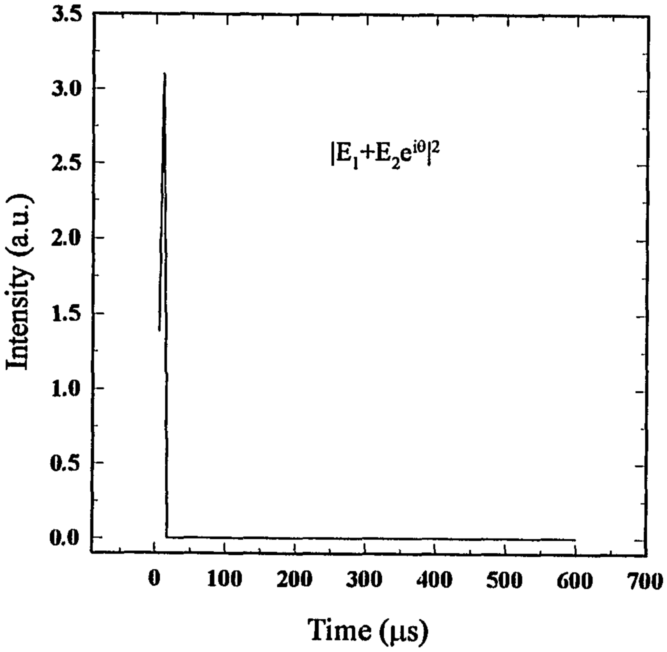

Figure 19 Calculated time series of $|E_1+E_2e^{i\theta}|^2$, corresponding to the intensity of the valley of the far-field with η_i not equal to zero.

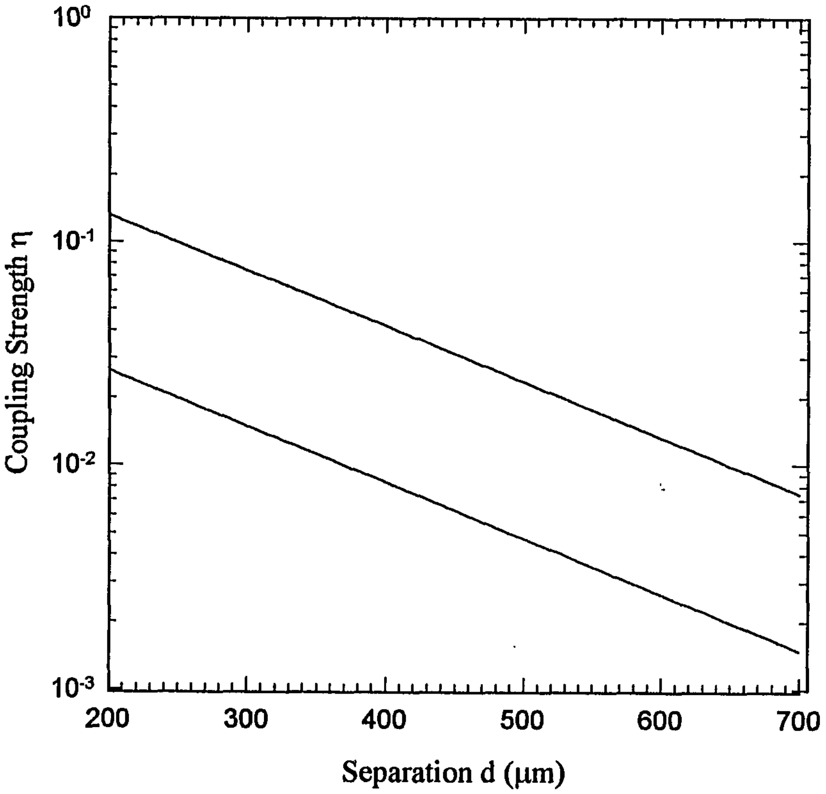

Figure 20 The calculated coupling strength between the two waveguides as a function of separation d.

of η_i and, to a much less degree, by η_r. If η_i is neglected, the calculated boundary of stable phase-locking for our experimental condition is plotted in Figure 21 line(a). The calculated detuning frequencies of stable phase locking are five orders magnitude smaller than the experimental values. In the vicinity of the boundary, there also exist a region in which the laser amplitude and phase exhibit irregular oscillations. If η_i is set to be $\Delta g/2g$, where Δg is the difference of the numerically calculated modal gains of the symmetric and antisymmetric supermodes, the calculated boundary of stable phase-locking, ranging from 23 MHz for $\eta_i = 0.1$ at $d = 300$ μm to 3 MHz for $\eta_i = 0.03$ at $d = 600$ μm, plotted in Figure 21 line(b). Compare with the theoretical calculation, the predicted detuning tolerance is one order of magnitude less than the observed.

Using the coupled-oscillator model, the magnitude of the electric fields in the two branches for a phase-locked mode are nearly equal, regardless of the detuning. Thus the far field pattern of the phase locked mode should be two lobed, at all times. This certainly can not account for the complex modal pattern in the transition region.

4.2 Re-examination of coupled-oscillator model

According to the coupled-oscillator model, phase locking is a result of phase synchronization between two oscillators. When the locking fails, the system becomes two individual elements, each operating in their respective frequencies with nearly equal amplitudes. Thus the state of operation is determined by the competition of four modes: the eigenmodes of the individual waveguides and the symmetric and antisymmetric modes of the composite waveguide.

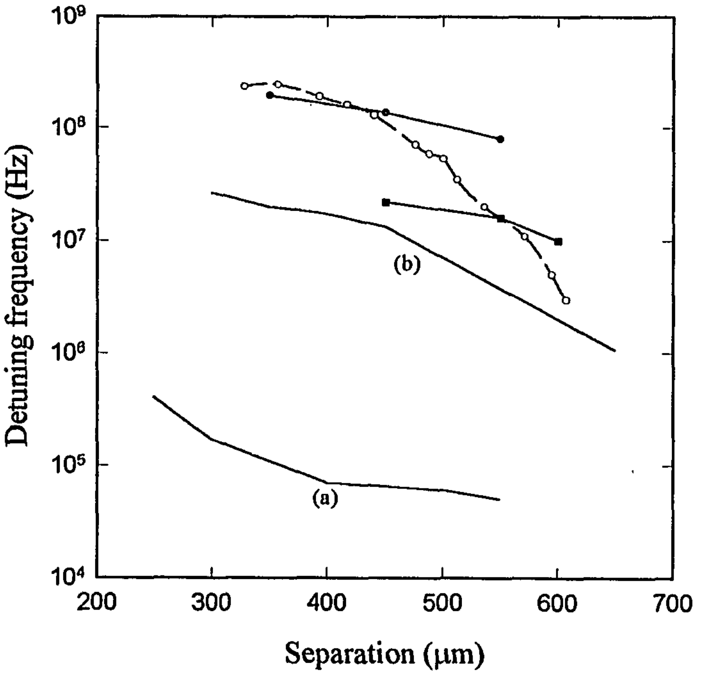

Figure 21 Calculated detuning frequency for the strong coupling (filled circles) and weak coupling (squares) regimes for comparison with the experimental data (open circles). the solid curve is calculated using coupled-oscillators equations.

The experimentally observed modal pattern and mode competition is certainly more complex than predicted by the coupled-oscillator model. For example, the three-lobed profile, shown in Figure 17(c), can not be synthesized by the linear superposition of two eigenmodes of the individual waveguides with equal amplitude. Thus we need to find an alternative approach to treat the problem of phase locking.

Our study reveals that a system of a two-element laser array with detuning, such as the one depicted in Figure 22, is not a two-mode system but can possess numerous eigenmodes each having a different frequency. The key point here is the detuning between the two arms due to the uneven length. Each arm has its resonance frequency. However, once the system is phase locked, there only exists one single frequency electric field. The question is: since the resonance frequency is differ from point to point along the transverse direction, at which frequency can the system be locked together.

In the following we will show that for a given frequency launches into the two-element array, there exists a distinct transverse distribution of the electric field and a characteristic modal gain. To quantitatively describe the electric-field profile, numerical calculation was carried out using the beam propagation method in an active waveguide. The laser is treated as a Fabry-Perot (F-P) etalon with gain. For an initial field of arbitrary amplitude and phase distribution, $Ee^{i\varphi}$, the waves undergo multiple bounces in the cavity. The number of bounces is determined by the mirror reflectivity of the F-P cavity. In the process of the propagation in the cavity, two effects must be taken into account. One is the amplification of the electric field in the gain media that must be considered if any active waveguide is simulated. Secondly, we must consider the Fabry-Perot effect by repeatedly

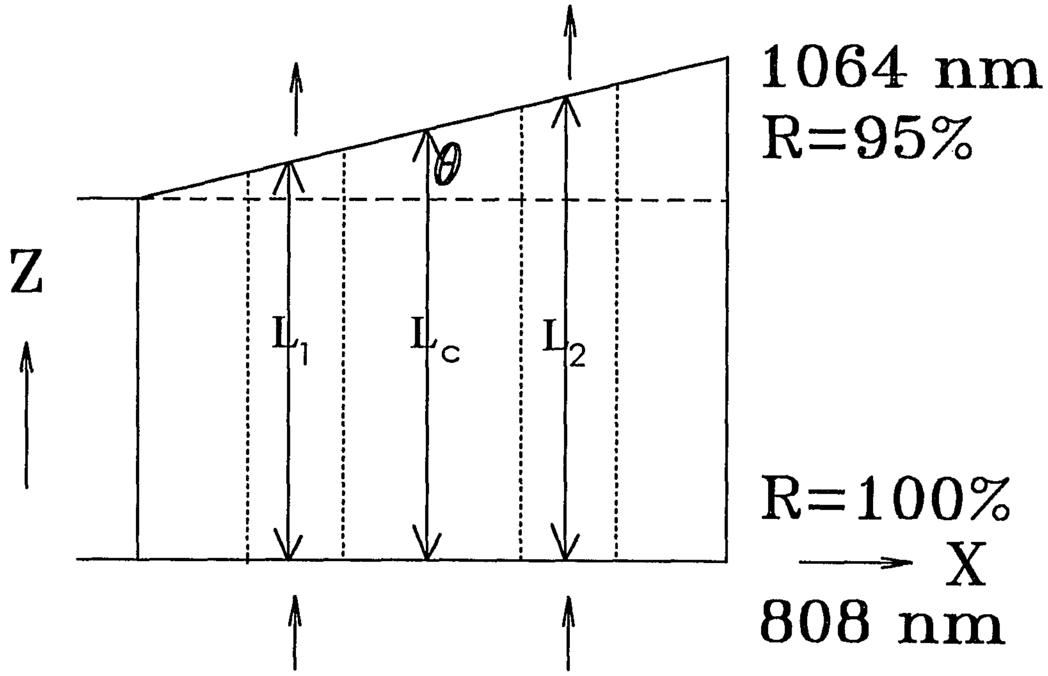

Figure 22 Schematic of a two-element laser array in a Nd:YAG etalon with a small wedge.

adding the electric field of earlier multiple bounces. These steps are crucial in determining the electric field in our situation due to the wedged etalon we used. At the branch where its cavity length is resonant with the frequency of the wave, the constructed interference occurs. In the branch where the given frequency does not match the frequency of the wave, the resultant electric field is partially canceled by an amount depending on the detuning frequency. The steady-state field is obtained by the summation of the output electric field over the coherence time as:

$$E(x) = \sum_{m} E_m e^{i\varphi_m(x)} (1 - r) e^{ikz(x)} e^{-mt/\tau} \tag{33}$$

where x is along transverse direction, z is longitudinal direction, E_m and φ_m are the amplitude and phase of electric field inside cavity after the m^{th} round trip, k is the wave number which is equal to an integer multiple of $2\pi/\lambda$ where the integer is chosen so that the wavelength corresponds to the peak of Nd:YAG gain curve, and τ is the photon lifetime. The factor $e^{-mt/\tau}$ (m is the integer, representing the number of round trips) is introduced to make the series convergent, since the addition of the electric field lasts over a period that is equal to the coherence time of the laser. The magnitude of the coherence time is equal to inverse of the laser linewidth. The laser linewidth measured from the spectrum analyzer is about 200 kHz, which corresponds to a coherence time of 30 μs.

Figure 23 illustrates the calculated near-field modal intensity patterns representing three different resonance conditions for an etalon with 15 MHz detuning between the elements. For the purpose of later discussion, only the antisymmetric modes with one node are generated for each frequency. The commonly known phase-locked mode, denoted as

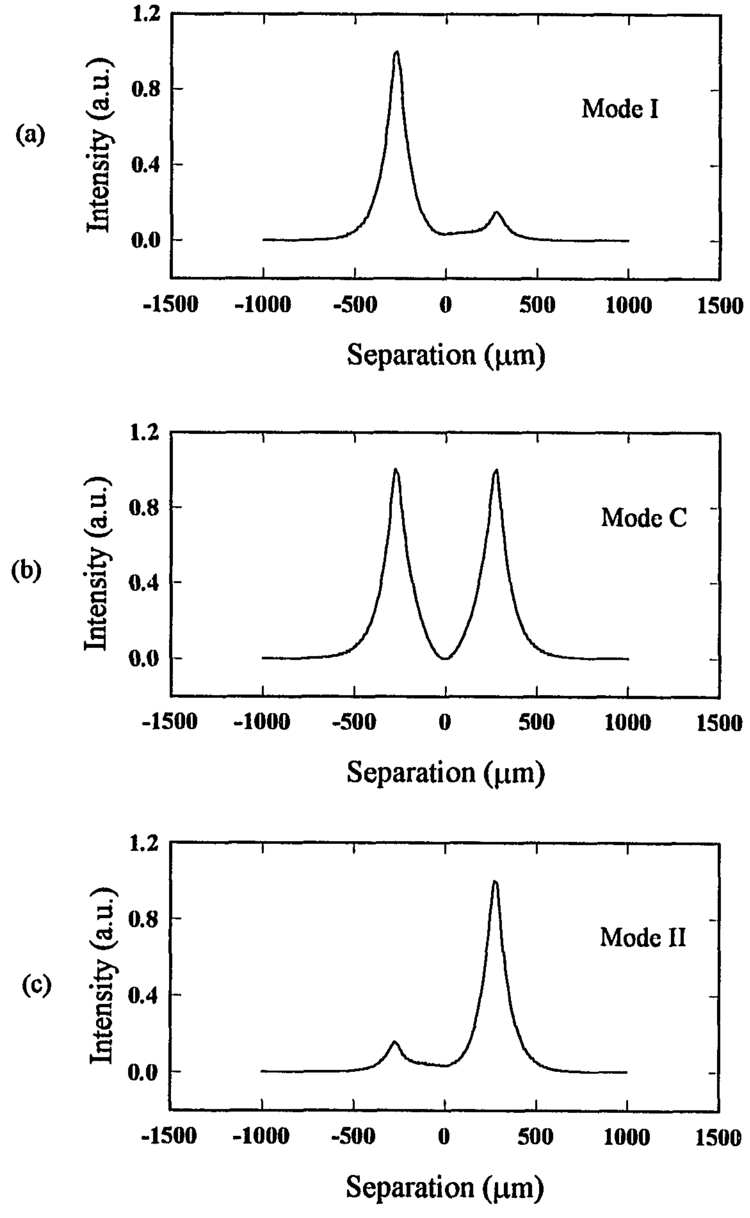

Figure 23 Calculated near-field patterns for waves resonant with (a) the left branch, (b) the composite waveguide, and (c) the right branch. The inter-element separation of 550 μm and detuning of 15 MHz.

mode C has a frequency that is resonant with the averaged cavity length $l_c \approx (l_I + l_{II})/2$ of the composite waveguide. The waves propagating in the two branches of the waveguide in the wedged etalon are slightly off resonance by an equal amount and the resultant fields in the two branches are equal in magnitude, as shown in Figure 23(b). For any other frequencies, the waves propagating in the two branches of the waveguide experience different interference conditions, resulting in an asymmetric field distribution. Modes I and II, in Figure 23(a) and 23(c), correspond to frequencies nearly resonant with the cavity lengths l_I and l_{II}, respectively. For the detuning frequencies of interest in our experiment, the difference in the length of the gain medium in the two branches is less than $10\,\mathring{A}$. Thus these two asymmetrical modes have nearly the same modal gain and can exist simultaneously, resulting in a beat wave at the detuning frequency.

The existence of these modal patterns was not appreciated before. The uneven intensity distribution can not be synthesized by using the coupled-mode equation with identical elements. If the detuning is sufficiently large, the waves propagating in the off-resonant branch experience large losses, and nearly all the intensity of modes I and II resides in one of the element, as shown in Figure 24 for a detuning of 350 MHz. These patterns resemble those predicted by the C-O model with identical elements.

As we have discussed above, taking the Fabry-Perot effect into account during the formation of the laser will result in a competition among the modes based on their modal gain. In the following, we will show that this competition model can fully explain the observed modal patterns and transitional behavior. The lasing mode is the eigen modes of the composite waveguide with the largest modal gain. (The modal gain is the imaginary part of the modal index.) Mode C is favored over Modes I and II if

$$exp\{2g_c(\Delta\omega)l\}R(1-\alpha_c(\Delta\omega)) > exp\{2g_i(\Delta\omega)l\}R(1-\alpha_i(\Delta\omega)) \quad \text{i= I, II} \qquad (34)$$

where g is the modal gain, l is the cavity length, R is the mirror reflectivity, α is the coupling coefficient per reflection at the mirror. Both g and α are functions of the detuning frequency, $\Delta\omega$. For small detuning frequencies, Mode C is favored owing to its higher modal gain. Depending on the detuning frequency at the boundary, two limiting regions are discussed separately as following.

1. Strong coupling

For small inter-element separations, the coupling coefficients can be as large as 0.1. The breaking of phase locking typically occurs at large detuning frequencies as we have discussed in section 3.4, the modal patterns of phase locked and unlocked modes are distinctly different. The competition took place among the eigen modes of distinctly different intensity distributions shown in Figure 24. The abrupt transition is due to the switching from Mode C, shown in Figure 24(b), which gives rise to a two-lobed far-field profile, to Modes I and II, shown in Figures 24(a) and 24(c), which give rise to a broad single-lobed far-field profiles. In this regime, modal gain of single-lobed profiles (Modes I and II) can be approximated by those of the single element laser. The effect of unequal length between the two elements created by the wedge angle of the etalon is to introduce a position-dependent phase shift across the wave front and accompanied loss after each round trip inside the cavity. Assuming that the phase shift occurs near the wedged mirror,

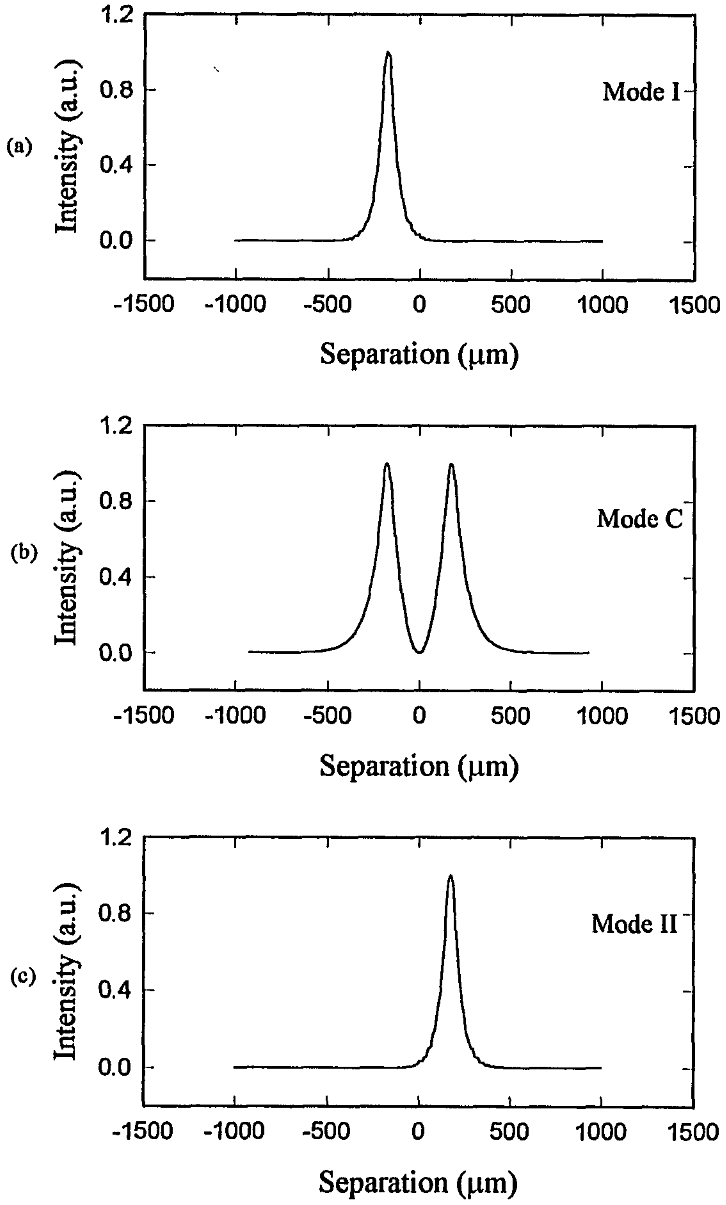

Figure 24 Calculated near-field patterns for wave resonant with (a) the left branch, (b) the composite waveguide, and (c) the right branch. The inter-element separation is 350 μm and the detuning frequency is 350 MHz.

the coupling coefficient $\alpha(\Delta\omega)$ upon reflection from the mirror can be calculated from the overlapping integral of the wavefunctions of the incident and reflected waves:

$$\alpha(\Delta\omega) = \left| \int \psi e^{i2k\Delta z(x)} \psi^* \, dx \right|^2 \tag{35}$$

where $\Delta z(x) = x\tan\theta$ and θ, the wedge angle, is related to the detuning frequency by $\Delta\omega = (\Omega\, d/l)\tan\theta$ where d is the separation between the two waveguides, Ω is the laser frequency, and l is the cavity length. For a given wedge angle, the coupling loss is larger for a beam with larger effective cross section. Thus the coupling loss, $1-\alpha$, of the Mode C increases more rapidly with the wedge angle than those of Modes I and II. The calculated loss, $(1-\alpha)$, as a function of wedge angle for various inter-element separation is shown in Figure 25. For sufficiently large wedge angle, the difference in the coupling loss can eventually offset the difference in the modal gain, resulting in switching of operation from mode C to modes I and II. In this calculation, the wavefunction of mode C is the eigen function of the waveguide and those of the mode I and II are approximated by the wavefunction of the individual waveguide. The calculated cross-over points, corresponding to the boundary of the phase locked and unlocked states, are plotted in Figure 21 by the solid line with filled circles. Hence in the regime of small inter-element separation, the calculated detuning frequencies at the boundary of phase locking are remarkably close to the experimental values for small inter-element separations considering that there is no adjustable parameters in the calculation. The calculated boundary for large inter-element separation deviates from the experiment data because, in

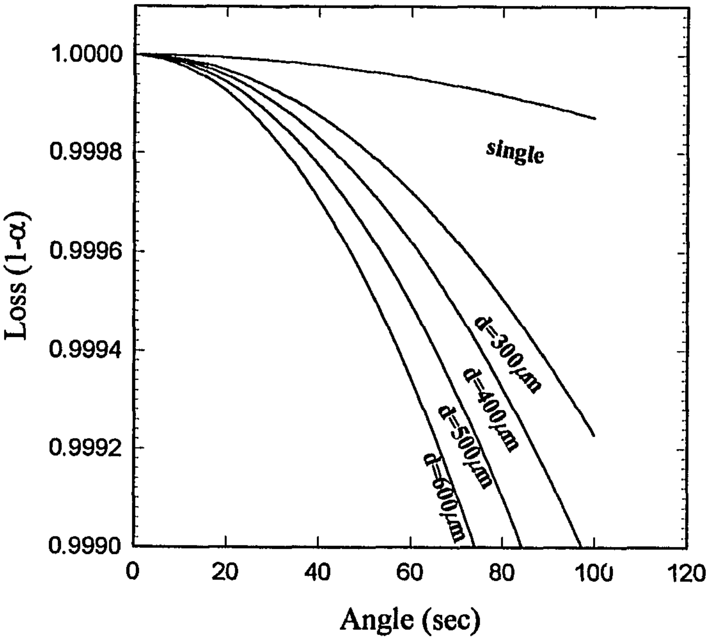

Figure 25 Calculated coupling coefficient (1-α) as function of wedge angle for various inter-element separations.

this regime, the approximation of the wavefunctions of modes I and II by those of the individual element is no longer valid. We will discuss it further in the following paragraph.

2. Weak coupling

For large inter-element separation, the breaking of phase locking occurs at small detuning frequencies. The modal competition near the boundary involves the type of modes shown in Figure 23. The same calculation described in the previous section indicates that, for a detuning frequency on the order of several MHz, the loss caused by the wave front tilt at the wedged mirror is negligible. This is also illustrated in Figure 25, (1-α) changes with wedge angle approximately in θ^2 and for θ in the range of 0-10 second, the loss is less than 2×10^{-5}. The main effect of increasing detuning is to cause changes in the modal gain due to redistribution of intensity between the two elements. To calculate the modal gain, the effect of a small detuning frequency in the Fabry-Perot cavity is assumed to cause a steady-state effective mirror reflectivity, γ, in each branch given by

$$\gamma = \frac{(1-r)^2}{1+r^2-2r\cos(2kd)} \tag{36}$$

where d is the cavity length, r is the reflectivity of the output coupler, k is the wave number. The γ factor is 1 for on resonance and is less than 1 for off resonance. The loss (1-γ) is then incorporated into the refractive index profile of the waveguide by adding $\delta n_i = \ln(\gamma)/4\pi\Gamma$ to the imaginary part of the refractive index steps where Γ is the overlapping integral of the modal intensity with the gain medium. The modified refractive-index profiles are then used for calculating the modal gains. For Mode C, the two branches experience the same loss,

$$\gamma_1 = \gamma_2 = \frac{(1-r)^2}{1+r^2-2r\cos(2kl_{I,II})},$$

the detuning results in a rapid decrease in the modal gain due to deviation from resonance in both branches. For Modes I and II,

$$\gamma_1 \cong 1,\ \gamma_2 = \frac{(1-r)^2}{1+r^2-2r\cos(2kl_{II})}$$

or vise versa, the effect of detuning is to shift the intensity from the element that is off-resonance toward the element that is closer to resonance, resulting a slower decrease in the modal gains with increasing detuning frequency. The calculated cross-over points are plotted by the solid line with triangles in Figure 21. This calculation predicts a much smaller tolerance of detuning in closer agreement with the experimental measurement. Furthermore, the features of the modal patterns in the vicinity of the transition can also be explained by this modeling. Figure 26 shows the calculated near-field and far-field modal patterns of the operating modes when the separation is increased for a given wedge angle. The phase-locked mode has a contrast ratio of 1 as shown in Figure 26(a). As the boundary is crossed, the onset of two independent asymmetric modes results in reduced contrast ratio, as shown in Figure 26(b). For larger separation, a three-lobed pattern occurs due to the intensity addition of two modes with highly uneven intensity distribution in the two elements as shown in Figure 26(c). For further increase in separation, a broader single-lobed profile is obtained as shown in Figure 26(d).

The absence of phase locking for separation greater than 600 μm can be attributed to the time-varying detuning which is comparable to the detuning tolerance. In our

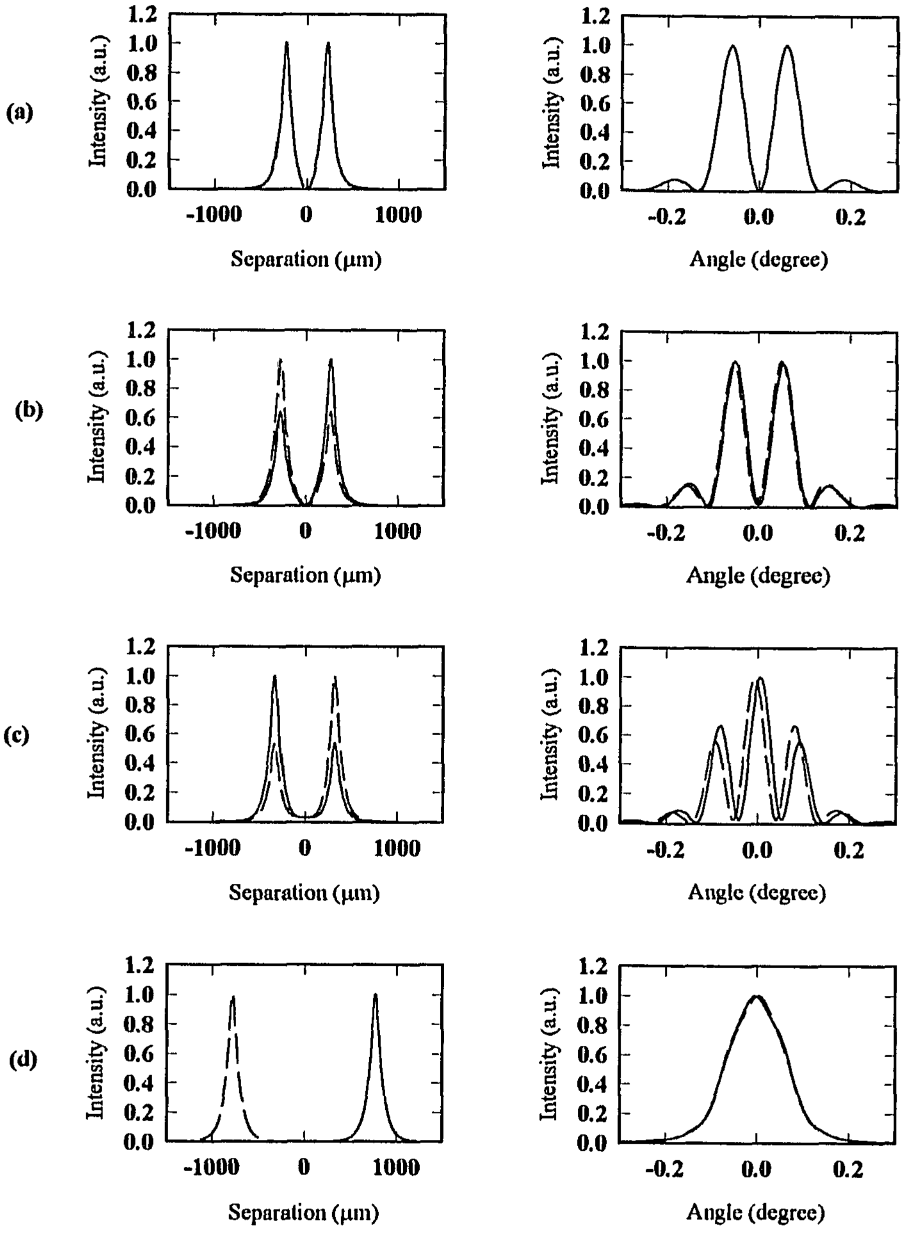

Figure 26 Calculated modal patterns of near-field and far-field of the dominant operating modes for various inter-element separations. The solid and dashed curves represent the eigen modes resonant with one of the elements of the composite waveguide.

experiment, the beat frequency of two unlocked laser has a short-term fluctuation of 1 MHz over a 1 ms period. This corresponds to a relative temperature variation of 3×10^{-4} K.

Chapter 5

Studies on semiconductor laser arrays and three-element solid-state laser arrays

5.1 Locking range of semiconductor laser arrays

Based on the understanding gained in the study of solid-state laser arrays, we now apply the same approach to analyze the locking range in semiconductor laser arrays in the presence of frequency detuning. This problem is of great practical importance and yet has not been investigated before.

In monolithic semiconductor laser arrays, the adjacent elements have the same physical cavity length. However, variations in temperature, carrier density, and stripe width caused by the uncertainty of microelectronic fabrication processes inevitably exist. For example, the red shift in lasing wavelength caused by increasing temperature is 0.05 nm/K. Thus a temperature difference of 0.01K between adjacent elements can cause a frequency detuning of 250 MHz.[32] Variation in the lateral dimension of waveguide can also causes variation in the oscillation frequency.

In the following, we will first establish the waveguide parameters for a typical semiconductor laser array.

(1) Real-part of the refractive index profile

In semiconductor lasers, the real part of the refractive-index profile is determined by the temperature gradient across the stripe and by the gradient of carrier density. The refractive index increases with increasing temperature and decreases with increasing carrier density. The combination of these two effects is quite complex. To simplify the analysis without losing generality, we will treat the case for pulsed operation and neglect the effect of heating. The real part of refractive index is then related to the carrier density through

$$\Delta n_r = -\alpha \Delta n_i$$

where Δn_r is the change of the real part of refractive index of gain media caused by the carrier-density fluctuation, Δn_i is the change of imaginary part of the refractive index, and α is phase-amplitude coupling constant. Since the carriers density is higher at the center of the stripe, the waveguide has an antiguiding (defocusing) effect for pulsed operation.

Consider a semiconductor laser created by optical pumping, the carrier density has a Gaussian-like distribution. For the sake of later discussion (current density rather than carrier-density is used by the reference curve), we equivalent the carrier-density into current-density, which satisfy the same distribution and can approximated by

$$N = N_0 e^{-4\ln 2\frac{(x-x_0)^2}{\sigma^2}} (A/cm^2) \qquad (37)$$

where N is current density, N_0 is the maximum density, σ is the Full-Width-Half-Magnitude (FWHM) and x_0 is the origin of x-coordinate(can be set to zero). According to our experimental condition, we choose the FWHM to be 7 μm and the threshold pumping current to be 100 mA. Therefore

$$\sigma = 7\mu m$$

$$N_0 = \frac{I}{S} = \frac{100mA}{7\mu m \times 500\mu m} \approx 2.8 \times 10^3 (A/cm^2)$$

where S is the cross-section area.

(2) The imaginary part of the refractive index profile

The relation between the gain and the current density does not follow a simple analytical relation. In quantum-well lasers, the gain typically increases following a linear relation for small current density (less than 121 A/cm^2) and following a parabolic function for current density greater than 121 A/cm^2. We approximate the gain-current density relation by

$$N = N_0 + bg + ag^2, \text{ when } g > 0$$

$$N = a' g + N_0 , \text{ when } g < 0$$

where N is the current density and g is the gain and a, b, a' are coefficients determined by curve fitting using the gain-current relation published in Ref [33]. Thus the above formula can be rewritten as:

$$g = 5.9\sqrt{N - 119} - 8.2 \text{ (1/cm)} \quad \text{for } N \geq 121.2 \text{ (A/cm}^2\text{)} \qquad (38)$$

$$g = 0.825N - 100 \text{ (1/cm)} \quad \text{for } N < 121.2 \text{ (A/cm}^2\text{)} \qquad (39)$$

By combining Equations (36) (37) and Equations (38) (39), the gain profile can be expressed as

$$g = 5.9\sqrt{2.8 \times 10^3 e^{-0.0566x^2} - 119} - 8.2 \text{ (1/cm)} \quad \text{for } N \geq 121.2 \text{(A/cm}^2\text{)} \qquad (40)$$

$$g = 0.825 \times 2.8 \times 10^{-3} e^{-0.0566x^2} - 100 \text{ (1/cm)} \quad \text{for } N < 121.2 \text{(A/cm}^2\text{)} \qquad (41)$$

The eigenmode of the waveguide is calculated numerically. The calculation is done by dividing the waveguide into 6 regions with linear ramp-type distribution. These ramp-type lines have end points, calculated by inserting the x_i into the above equations, at

lateral distance (x μm)	Imaginary of index (Δn_i)
3.5	3×10^{-4}
0	2.1×10^{-4}
-4	0
-7	-3.3×10^{-4}
-7	-3.4×10^{-4}

This imaginary part of refractive index is shown in Figure 27(a). The corresponding Δn_r is plotted in Figure 27(b) for $\alpha = 1$.

The refractive index profile of the waveguide for the two-element semiconductor laser array is shown in Figure 28. As shown in Figure 27, the individual element is an "gain-guided" antiguide laser. When two antiguide lasers are placed in closed proximity to each other, the region between the elements becomes a "waveguide" which draws the modal field away from the gain region and thereby reduces the modal gain. For larger separation, the field distribution of the eigenmode of the composite waveguide can be highly distorted with most of the energy propagating outside the gain region. Two examples of the modal field distribution for two different separations are illustrated in Figure 29. The antiguiding results in a rapid decrease in the modal gain as the inter-element separation is increased.

As discussed in section 4.2, the effect of frequency detuning between the two branches of the waveguide is to introduce a larger effective mirror loss to the branch

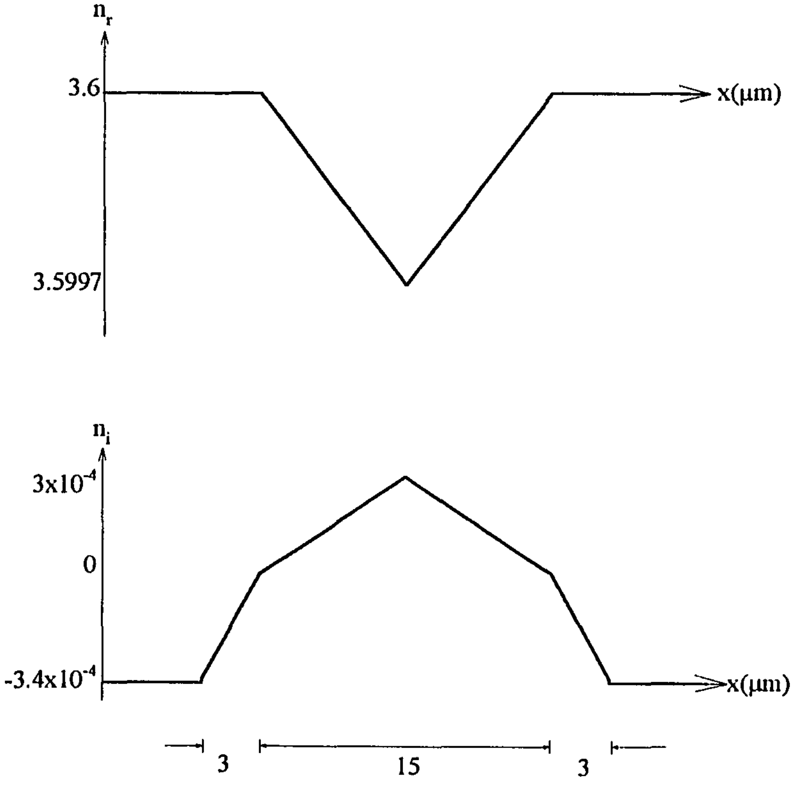

Figure 27 Refractive-index profiles for an "gain-guided" antiguide laser.

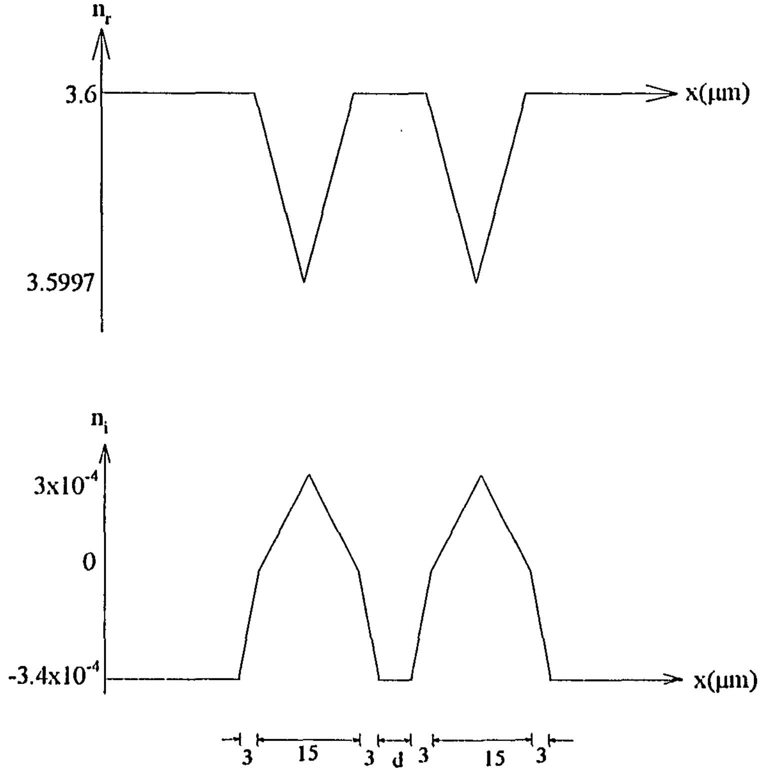

Figure 28 Refractive-index profiles for a two-element "gain-guided" laser array. d is the separation between two elements.

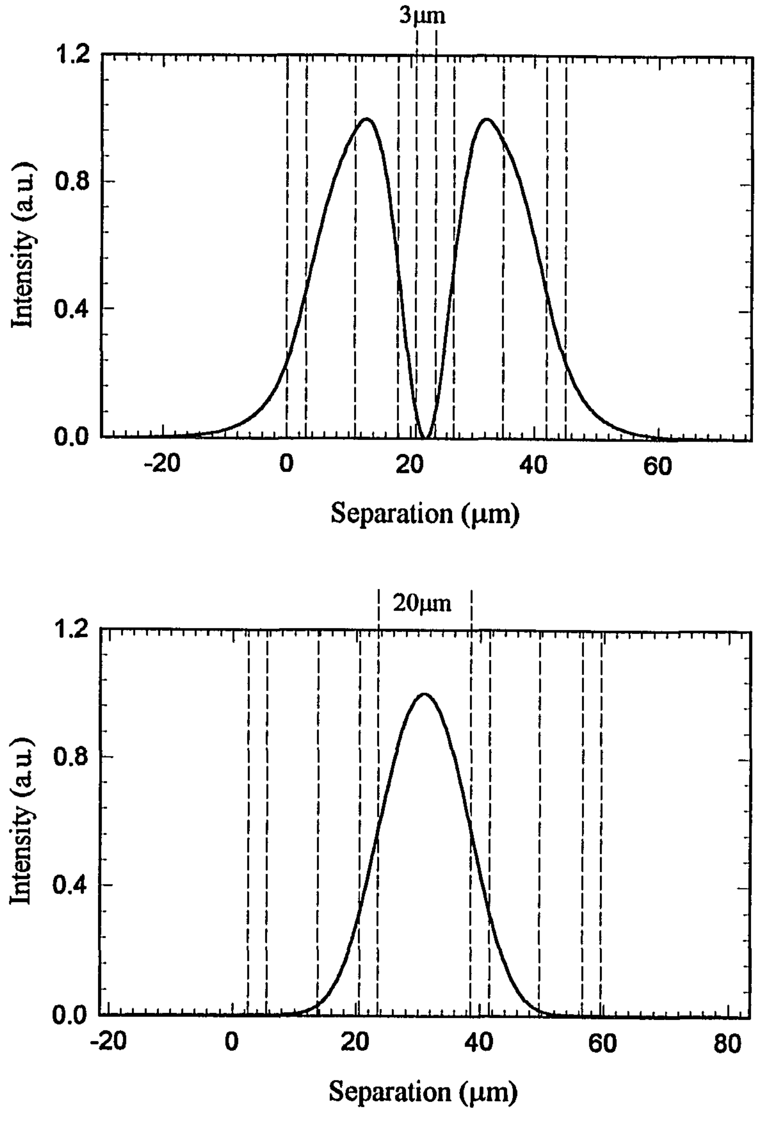

Figure 29 Modal Profile of two-element semiconductor antiguide laser array. Separation between two elements are (a) 3 μm and (b) 20 μm.

whose frequency does not match the frequency of the wave. The loss (1-γ) is then incorporated into the refractive-index profile of the waveguide by adding $\delta n_i = ln\gamma / 4\Gamma$ to the imaginary part of the refractive index steps and by subtracting $\alpha \times \delta n_i$ from the real part of the refractive index steps where Γ is the overlapping integral of the modal intensity with the gain medium. The modified refractive-index profiles are then used for calculating the modal gains. The calculated boundary for phase locking in the detuning vs separation space are plotted in Figure 30. The largest detuning frequency such system can tolerant is 30 GHz and it decreases rapidly to zero. The cut-off is mainly caused by the distortion of the modal profile in the antiguide laser array when most of the modal energy is pulled toward the region between the gain region. Thus although the coupling strength is still quite large, "phase-locked mode" is not favored due to reduced overlapping with the gain regions.

5.2 Modal behavior of a three-element laser array with parallel coupling

The study of phase locking is extended to a three-element laser array. The three-element array is of interest because, according to theoretical predictions based on the C-O model, it was unstable and could not form a phase locked mode due to the large number of dynamic variables in the system[14]. The three elements can be arranged to form a linear array with series coupling in which the coupling takes place between adjacent elements, or

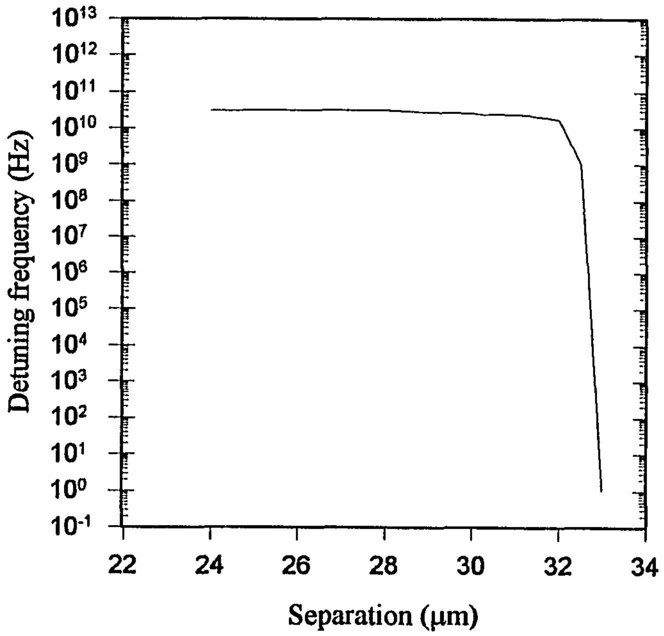

Figure 30 The detuning frequency versus separation for two-element antiguide semiconductor array.

a triangular array with parallel coupling in which each element is coupled to every other elements in the system. We have studied the triangular array, as shown in Figure 31.

The experimental setup is similar to that shown in Figure 10 except that a third semiconductor laser is added as the pump source and the Nd:YAG etalon is 1-mm thick.

A three-element laser array with parallel coupling is expected to have two eigenmodes with minimum coupled intensity characterized by phase difference of 2π/3, and -2π/3. These two configurations can be explained as following. The Gaussian-like field amplitude g_n with unit mode radius centered on (x_{n0}, y_{n0}) is given by

$$g_n = \sqrt{\frac{2}{\pi}} a_n \exp[i(\omega t + \phi_n)] \exp[-(x - x_{n0})^2 - (y - y_{n0})^2] \tag{42}$$

where a_n is real amplitude constant and ϕ_n is the phase. Assuming that the intensity for all modes is unit and the distance between the elements is $2d$. The intensity of the superposition of the three elements can be expressed as

$$\begin{aligned} I_c(d) &= \int_{-\infty}^{\infty} dx \int_{-\infty}^{\infty} dy |g_1 + g_2 + g_3|^2 \\ &= 3 + 2\exp[-2d^2]\{\cos(\phi_1 - \phi_2) + \cos(\phi_2 - \phi_3) + \cos(\phi_3 - \phi_1)\} \end{aligned} \tag{43}$$

Defining the phase difference between elements Δ_i as,

$$\begin{aligned} \Delta_1 &= \phi_1 - \phi_2 + 2n_1\pi \\ \Delta_2 &= \phi_2 - \phi_3 + 2n_2\pi \\ \Delta_3 &= \phi_3 - \phi_1 + 2n_3\pi \end{aligned} \tag{44}$$

where n_i denotes arbitrary integer.

The minimum can be found by setting the partial derivatives of coupling intensity to zero. Namely,

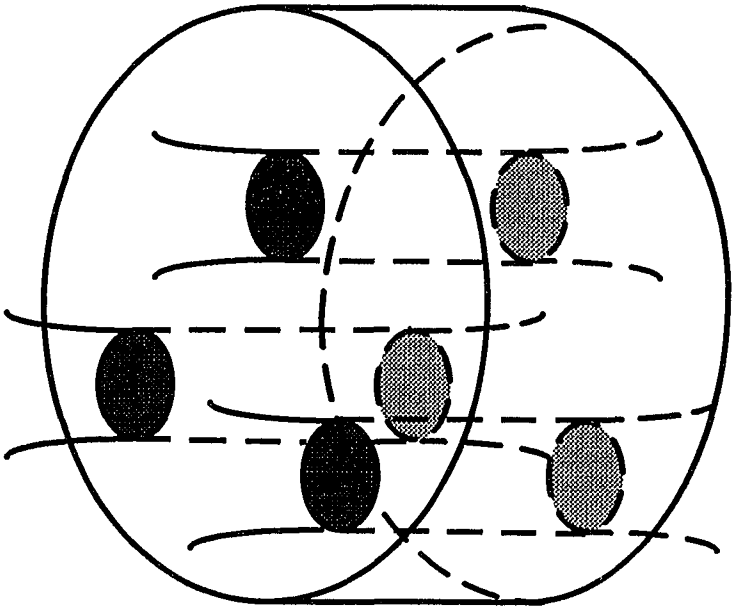

Figure 31 Schematic of the three-element laser array.

$$\begin{aligned} \frac{\partial I_c}{\partial \Delta_1} &= -2\exp[-2d^2](\sin\Delta_1 - \sin\Delta_3) = 0 \\ \frac{\partial I_c}{\partial \Delta_2} &= -2\exp[-2d^2](\sin\Delta_2 - \sin\Delta_3) = 0 \end{aligned} \tag{45}$$

Equation (45) is satisfied by either

$$\Delta_1 = \Delta_2 = \Delta_3 = \pm\frac{2\pi}{3}, 0, \pi$$

or, any combination of 0, π, π for Δ_i. (One of the Δ_i is 0 and the other two are π). It is obvious that $\pm 2\pi/3$ gives the minimum coupled intensity. The coupled intensity is proportional to the laser output from the cavity, and also proportional to the input. So minimization the coupled intensity means that the lowest threshold is achieved. From this consideration, the mode with $2\pi/3$ or $-2\pi/3$ phase relation is most favored due to the highest gain. The spatial patterns for $\pm 2\pi/3$ are same.

As the first order approximation, we assume that the electric field in each element has a Gaussian distribution and the modal field of the laser array is produced by linear superposition of eigenmodes of a fixed phase difference. We assume the three individual lasers are identical, each with field amplitude E_0 and waist ω_0. The far-field intensity at any point (x, y, z) in space can be expressed as following:

$$E(x,y,z) = \sum_{i=1}^{3} E_0 \frac{\omega_0}{\omega(z)} \exp\{-j[kz - \eta(z)] - r_i^2[\frac{1}{\omega^2(z)} + \frac{jk}{2R(z)}]\} e^{j\theta_i} \tag{46}$$

where $\omega^2(z) = \omega_0^2(1 + \frac{z^2}{z_0^2})$

$$\eta(z) = \tan^{-1}(\frac{z}{z_0})$$

$$R(z) = z(1 + \frac{z^2}{z_0^2})$$

$$r_i = \sqrt{x_i^2 + y_i^2 + z_i^2}$$

$$z_0 = \frac{\pi\omega_0^2 n}{\lambda}$$

$$k = \frac{2\pi}{\lambda}$$

Shown in Figure 32 is the calculated far-field pattern corresponding to phase relation of $2\pi / 3$. The parameters used in Figure 32 are $\omega_0 = 200$ μm, z=100 cm, and λ=1.06 μm.

Shown in Figure 33 is our experimentally observed far-field pattern of three-element parallel coupled laser array. The pattern is donut shaped with the center in total darkness, indicating that it is the mode with phase difference $2\pi/3$.

Although the near- and far-field patterns are rather stable and reproducible, the polarization of the pattern as viewed through a linear polarizer is unstable. Various polarization states, from nearly linearly polarized state to other undetermined polarization states, have been observed from time to time. We attribute this unstable polarization property of the system to the sensitivity to external perturbation in the three-element system. Unlike the two-element system, in which a preferred interaction axis lies along the line connecting the two elements, three-element system with parallel coupling do not have a preferred axis. Therefore any inadverdently introduced and time varying perturbations, such as detuning, uneven temperature distribution, and pumping energy etc. between the elements, could easily break the symmetry and determine the momentarily polarization states.

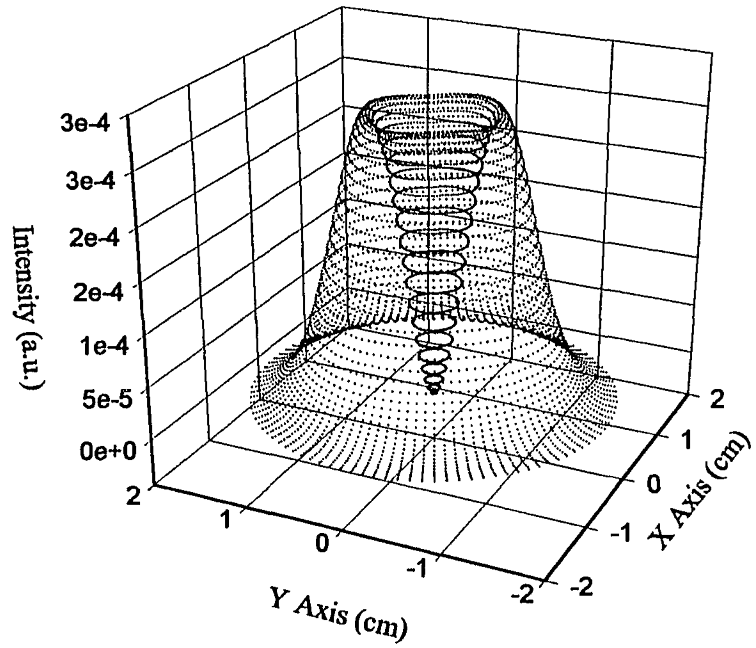

Figure 32 Calculated far-field patterns of a three-element phase-locked Nd:YAG laser array The phase difference between the elements is 2π/3.

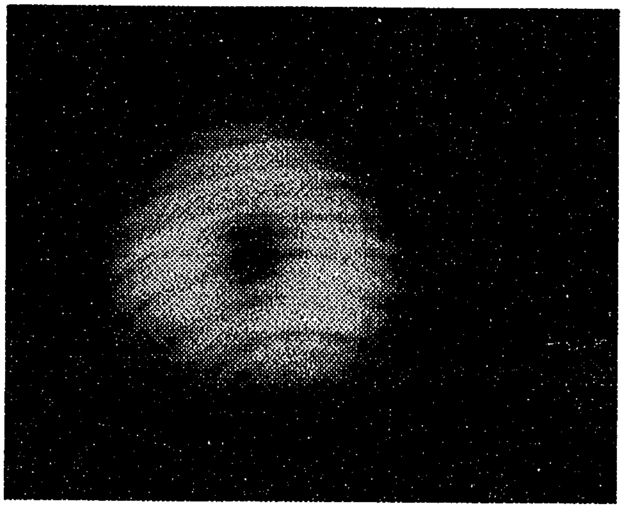

Figure 33 Photograph of far-field pattern of three-element parallel coupled laser array

Chapter 6

Summary and Conclusion

This study was motivated by the various interesting predictions of optical instability and nonlinear dynamics in laser arrays. These predictions were based on the calculation by treating the laser arrays as a coupled oscillators. We hoped that, using a controlled experimental condition, the dynamics of phase-locking can be observed as a test of the coupled-oscillator model.

We have used a two-element laser array as a testing model for studying the mechanism of phase locking in an evanescent-coupled laser array. The two-element laser array is created in a monolithic Nd:YAG etalon by photo-pumped with two quantum-well diode lasers. With the photo-pumping technique, the separation and frequency detuning between the two elements can be controlled and continuously varied for a wide range of coupling strength. We also studied the tolerance of frequency detuning in the array using a Nd:YAG etalon with a wedged angle that allows us to create a controllable frequency difference between the elements.

We found discrepancies between the experimental results and theoretical predictions. According to previously published calculations based on the coupled-oscillator model, the phase locking time in the Nd:YAG laser system is on the order of 300 μs. Our experiment reveals that the phase locking is as fast as the on-set of lasing (<1 μs) without any observable slow evolutionary process. The experimental data also show that the frequency detuning for phase locking is five-order of magnitude larger than calculated from the original coupled-oscillator model which was done without introducing the imaginary part of coupling strength. Although the calculated phase locking time can be reduced and the magnitude of the frequency detuning for phase locking increased by taking into account the imaginary part of the coupling strength, the range of phase locking still can not be explained by the coupled-oscillator model. The observed modal behavior in the vicinity of the boundary between phase locked and unlocked regions is, by far, much more complex than predicted by the coupled-oscillator model. We have also observed modal pattern that can not be synthesized by the linear superposition of the electric fields of the eigenmodes of the individual waveguide. These disagreements call for re-examination of the coupled-oscillator approach.

Based on the coupled-oscillator model, the temporal evolution of the eigenmodes of a two-element laser array is described by the linear superposition of two eigenmodes of the individual elements whose temporal behaviors are governed by the rate equations. For a given initial condition, the time series of the electric field is deterministic.

Our analysis shows that a two-element laser array is not a two-mode system and can not be adequately described by superposition of the two eigenmodes of the individual elements. In fact, a two-element laser array can possess numerous eigenmodes, each having a different frequency. Our numerical calculation shows that, for a wave of a given frequency launched into the two-element waveguide laser array, the steady-state magnitude of the electric field in each element is determined by the resonance condition in that element. The commonly known symmetric and antisymmetric modes are special cases when the frequency of waves is such that the resonance conditions in the two branches are identical. When the resonance conditions in the two branches are not identical, the field magnitudes in the two branches are not the same, resulting in various modal patterns, such as the three-lobed far-field patterns, that can not be synthesized by the coupled-mode calculation.

Based on this new understanding, we have carried out numerical calculations for the modal patterns and the tolerance of frequency detuning in the two-element laser array with a detuning. The agreement between the theory and experiment is remarkable.

We have also analyzed the modal behavior in a gain-guided two-element semiconductor laser array. The gain-guided array, most commonly used structure in semiconductor laser arrays, has a negative real part of refractive index step, under the stripe. In a gain-guided "antiguide" laser, considerable modal distortion can arise as the separation between elements increased. We have shown that distortion results in reduction in the modal gain of the phase locked state. Thus phase locking can be broken although the "coupling" between the elements is still large. This is an example that a large coupling strength between the elements does not always guarantee phase locking.

An important implication from the new understanding achieved in this study is that the dynamics in a laser array is not a deterministic process. The temporal instability as predicted by coupled rate equations can result in a temporal variation in the modal gain of the launched field to become either higher or lower than the steady state value. When the modal gain is momentarily lower than the steady state value, the onset of more favorable modes, which are not eigenmodes of the coupled-oscillator equations with different frequencies, whose profiles overlap better with the gain profile can overpower the nonlinear dynamics predicted based on the deterministic model. Indeed, throughout this study, we have found no experimental evidence of optical instability in laser arrays.

Reference

1 M. Teneya, M. Matsumoto, S. Matsui, S. Yano, and T. Hijikata, "0° phase mode operation in phased-array laser diode with symmetrically branching waveguide", Appl. Phys. Lett., **47**, 341(1985).

2 J. P. Hohimer, G. R. Hadley, and A. Owyoung, "Interelement coupling in gain-guided diode laser arrays", Appl. Phys. Lett., **48**, 1504(1986).

3 J. R. Leger, M. L. Scott, and W. B. Veldkamp, "Coherent addition of AlGaAs lasers using microlenses and diffractive coupling", Appl. Phys. Lett., **52**, 1771(1988). See also, J. R. Leger and G. J. Swanson, Opt. Lett., **15**, 288(1990).

4 N. W. Carlson, G. A. Evans, J. M. Hammer, M. Lurie, J. K. Butler, S. L. Palfrey, M. Ettenberg, L. A. Carr, F. Z. Hawrylo, E. A. James, C. J. Kaiser, J. B. Kirk, W. F. Riechert, J. R. Shealy, J. W. Sprague, S. R. Chinn and P. S. Zory, "Dynamically stable 0° phase mode operation of a grating-surface-emitting diode-laser array", Opt. Lett., **13**, 312(1988).

5 D. Scifres, R. Burnham, and W. Streifer, "Phase-locked semiconductor laser array", Appl. Phys. Lett., **33**, 1015(1978).

6 M. Orenstein, E. Kapon, J. P. Harbison, L. T. Florez, and N. G. Stoffel, CLEO'91, (1991) Paper JThA6.

7 M. Oka, H. Masuda, Y. Kaneda, and S. Kubota, "Laser-diode-pumped phase-locked Nd:YAG Laser arrays", IEEE J. Quantum Electron., QE-**28**, 1142(1992).

8 M. Jansen, J. J. Yang, S. S. Ou, J. Wilcox, D. Botez, L. Mawst, and W. W. Simmons, CLEO'89 (1989) Paper FL2.

9 F. X. D'amato, E. T. Siebert, and C. Roychoudhuri, CLEO'89 (1989) Paper FL3.

10 D. R. Scifres, W. Streifer, and R. D. Burnham, "Experimental and analytic studies of coupled multiple stripe diode lasers", IEEE J. Quantum Electron., QE-**15**, 917(1979).

11 D. Botez, "Array-mode far-field patterns for phase-locked diode-laser arrays: coupled-mode theory versus simple diffraction theory", IEEE J. Quantum Electron., QE-**21**, 1752(1985).

12 J. K. Butler, D. E. Acklley, and D. Botez, "coupled-mode analysis of phase-locked injection laser arrays", Appl. Phys. Lett., **44**, 293(1984).

13 T. L. Paoli, W. Streifer, and R. D. Burnham, "Observation of supermodes in a phase-locked diode laser array", Appl. Phys. Lett., **45**, 217(1984).

14 K. Otsuka, Phys. Rev. Lett., "Self-induced phase turbulence and chaotic itinerancy in coupled laser systems", **65**, 329(1990).

15 H. G. Winful, and L. Rahnman, "Synchronized chaos and spatiotemporal chaos in arrays of coupled lasers", Phys. Rev. Lett. **65**, 1575(1990).

16 S. S. Wang, and H. G. Winful, "Dynamics of phase-locked semiconductor laser array", Appl. Phys. Lett., **52**, 1774(1988).

17 S. S. Wang, and H. G. Winful, "Stability of phase locking in a coupled semiconductor laser arrays", Appl. Phys. Lett., **53**, 1894(1988).

18 R. K. Jakobsen, R. A. Indik, J. V. Moloney, A. C. Newell, H. G. Winful, and L. Raman, "Diode-laser array modes: discrete and continuous models and their stability", J. Opt. Soc. Am., **B8**, 1674(1991).

19 G. A. Wilson, R. K. DeFreez, and H. G. Winful, "Modulation of phased-array semiconductor lasers at K-band frequencies", IEEE J. Quantum Electron., QE-**21**, 1696(1991).

20 R. A. Elliot, R. K. Defreez, T. L. Paoli, R. D. Burnham, and W. Streifer, IEEE J. Quantum. Electron., QE-**21**, 598(1985).

21 D. Scifres, R. D. Burnham, W. Streifer, and M. Bernstein, "Lateral beam collimation of a phased array semiconductor laser", App. Phys. Lett. Vol **41**, 614, 1982.

22 D. Botez, and J. C. Connolly, "High-power phase-locked arrays of index-guided diode lasers", App. Phys. Lett. Vol **43**, 1096(1983).

23 J. K. Butler, D. E. Ackley, and D. Botez, "Coupled-mode analysis of phase-locked injection laser arrays", App. Phys. Lett., Vol **44**, 293(1984).

24 E. Kapon, J. Katz, and A. Yariv, "Supermode analysis of phase-locked arrays of semiconductor lasers", Opt. Lett., Vol **10**, 125(1984).

25 S. R. Chinn, and R. J. Spiers, "Modal gain in coupled-stripe lasers", IEEE J. Quantum Electron., QE-**20**, 358(1984).

26 A. Yariv, *Quantum Electronics*, 3rd ed, John Wiley & Sons, New York, 1989, chapter 22.

27 H. G. Winful, S. S. Wang, and R. K. DeFreez, OSA proceedings on Nonlinear dynamics in optical systems, Vol 7, P. 119(1990).

28 W. Koechner, *Solid State Laser Engineering,* Springer-Verlag, New York, 1992, pp51.

29 A. G. Fox and T. Li, IEEE J. Quantum Electron., QE-**4**, 460(1968).

30 G. P. Agraw, N. K. Dutta, *Long wavelength semiconductor lasers*, 1st ed., Van Nostrand Reinhold, 1986.

31 A. G. Fox and T. Li, Bell Sys. Tech. J. **40**, 453(1961).

32 GHB Thompson, *physics of semiconductor laser devices*, John Wiley & Sons, New York, 1980, pp517.

33 S. R. Chinn, P. S. Zory, and A. R. Reisinger, "A model for GRIN-SCH-SQW Diode Lasers", IEEE J. Quantum Electron., QE-**24**, 2191(1988).

34 Jingwen Xu, Shiqun Li, K. K. Lee and Y. C. Chen, "Phase locking in two-element laser array: a test of the coupled-oscillator model", Opt. Lett. Vol **18**, 513 (1993).

35 Jingwen Xu, K. K. Lee, and Y. C. Chen, "Phase locking in a two-element laser array with detuning", Opt. Commun., vol **105** (1995).

36 Jingwen Xu, Shiqun Li, K. K. Lee, and Y. C. Chen, "Phase locking of a two-element laser array", Proceedings ICLOE'92, SPIE vol **1979**, 124 (1993).